DEVELOPMENTS IN MOIRE INTERFEROMETRY: CARRIER PATTERN TECHNIQUE AND VIBRATION INSENSITIVE INTERFEROMETERS

by

Yifan Guo

Dissertation submitted to the Faculty of the
Virginia Polytechnic Institute and State University
in partial fulfillment of the requirements for the degree of
DOCTOR OF PHILOSOPHY
in
Engineering Mechanics

APPROVED:

R. Czarnek, Chairman	D. Post
C. W. Smith	J. Morton
D. Mook	R. O. Claus

February, 1989

Blacksburg, Virginia

DEVELOPMENTS IN MOIRE INTERFEROMETRY: CARRIER PATTERN TECHNIQUE AND VIBRATION INSENSITIVE INTERFEROMETERS

by

Yifan Guo

R. Czarnek, Chairman

Engineering Mechanics

(ABSTRACT)

Due to the rapid expansion of applications of composite materials, investigations of their properties have greatly increased. Since theoretical and numerical methods have many limitations for anisotropic materials, experimental methods are sometimes the only way to answer the questions. It has been proved that moire interferometry is a powerful technique in the study of composite materials.

The high sensitivity and resolution of a measurement technique is the key to determining the properties of a material which has a fine and complicated structure such as fiber-reinforced composite laminates. In this paper, a carrier fringe method is introduced to increase the resolution of the fringe gradient in the moire technique. The ability of measurement is extended to the micromechanics region. High strain concentrations and the dramatic displacement variations can be determined by measuring the slopes of carrier fringes. Strain distributions across the plies (with the thickness of 125 μm) in graphite/epoxy composites and strain concentrations in the resin-rich zones (with the thickness of 10 μm) between neighboring plies are revealed by the carrier fringe technique. Three experiments are presented to show the effectiveness of the application of carrier fringes to resolve fringe gradients and obtain strains.

The current moire technique is limited to the optical laboratory because it is extremely sensitive to the disturbance of the environment. A vibration with magnitude of 0.2 μm can completely wash out the contrast of a moire fringe pattern. The study has been done in moving moire interferometry off the optical table. Vibration insensitive moire systems are investigated to extend the moire technique to the tests of large structures and using testing machines for loading. Vibration problems are discussed and the new ideas for eliminating vibration effects are presented. Six representative schemes are analyzed and three of these systems are built to perform experiments in rough environments such as on a hydraulic testing machine. The results show the great success of these new systems.

Acknowledgements

The author wishes to express his thanks to Prof. Robert Czarnek, who as the chairmen of the committee offered a great many ideas and advice during the research and the writing of the dissertation. Also thanks to his wife, , for her constant concern and encouragement.

Great appreciation is expressed to Prof. Daniel Post, who as the group leader first led the author to the wonderful land of photomechanics and kept providing and sharing his intelligence and talent. The constant spiritual support and the help for a long period from Prof. Daniel Post and his wife was indispensable for the author to complete his work in VPI & SU.

In addition, thanks to:

- Prof. R. Claus in Electrical Engineering for his help in fiber optics and suggestions for the dissertation, and other professors who served on the committee.

- for her help in improving the writing.

• , and all other members in the Photomechanics Group who helped a great deal in the experiments.

Table of Contents

1.0 Introduction

In recent years, composite materials have been used in numerous products because of their high performances and light weight. These applications include use in space vessels, aircraft, ships and automobiles and have proved that composite materials can be used to replace metals in most cases and give better performance. However, there exist many questions about the mechanical properties of composite materials. Although more work and people are involved and more money is spent on research and the manufacture of composite materials, many problems remain unsolved and many parameters need to be investigated [1,2].

Of the various types of composite materials, the fiber-reinforced composites with lamination structure are the most popular for high technology applications [3]. This kind of composite usually has a very complex structure. The fiber diameter is less than 10 micrometers for graphite fiber, and the thickness of a ply is typically about 125 micrometers in graphite/epoxy composites. For a good understanding of the mechanical properties, the micromechanics study has to be applied. So far, theoretical and numerical analyses are frequently unsatisfactory since their accuracy largely depends on how well the phenomenological behavior is known. Experimental methods are necessary for

the investigation of the properties of composite materials and for the study of composite structures. Among all the existing experimental methods, few of them can be possibly used in the micromechanics study for such complicated structures.

Moire interferometry has certain unique advantages and has been successfully used to investigate properties of composite materials [4,5,6]. Examples include studies of nonuniformities in composite materials [7], strain concentrations on notched composite specimens [8], edge effects of laminated composites [9], thermal strains in composites [10,11], shear properties in the individual plies and interlaminar shear strains [12,13], strain concentrations in composites with an embedded optical fibers [14], compression properties [15], two body contact stress problems in composites [16] and strain variations in metal-matrix composites [17,18,19]. It has been proved that moire interferometry, with its sensitivity and resolution, can solve many problems in macromechanics. In addition, moire interferometry can now be applied to micromechanical measurements when the microstructure is relatively coarse. For many problems, it is superior to all the other electronic and optical methods of displacement measurement.

Moire interferometry is an interferometric method and requires a strong coherent light. High quality optics must be used to eliminate the optical aberrations. Experiments usually have to be performed on an optical table and in an optical laboratory in order to isolate the apparatus from vibrations. All these requirements make the technique fairly expensive and complicated. As a new technique, moire interferometry needs to be developed and improved to meet the demands of new problems as they arise.

1.1 Moire Interferometry

Moire interferometry is an optical technique of displacement measurement, which combines the whole-field method with very high sensitivity and resolution [20]. Compared to other mechanical, optical and electronic methods which have only one or two of these advantages, moire technique is very unique and significantly advanced [21]. Moire interferometry is extremely powerful for shear strain measurement. For example, Fig. 1-1 shows a fringe pattern (y-displacement field) obtained by moire interferometry from a metal-matrix composite specimen with a central slot. The whole-field shear strain distribution, with high strain concentrations, can be determined by extracting data from this fringe pattern and the corresponding x-displacement field. No other method can compete in this application.

1.1.1 Basic principles

Displacement measurements of a deformable body are the determination of the changes of positions of its points. To determine the changes of the positions, one has to mark the object and to use a reference scale like a ruler. In geometric moire and moire interferometry, the marks are constructed by the specimen grating and the scale is the reference grating.

Figure 1-2 shows the geometric moire method. Basically, this method uses the reference grating to measure the changes of the specimen grating. Before the deformation, the specimen grating and the reference grating have the same frequency. By superimposing these two gratings, a null-field, which simply means no difference in frequency and direction between these two gratings, can be obtained. After the deformation, the

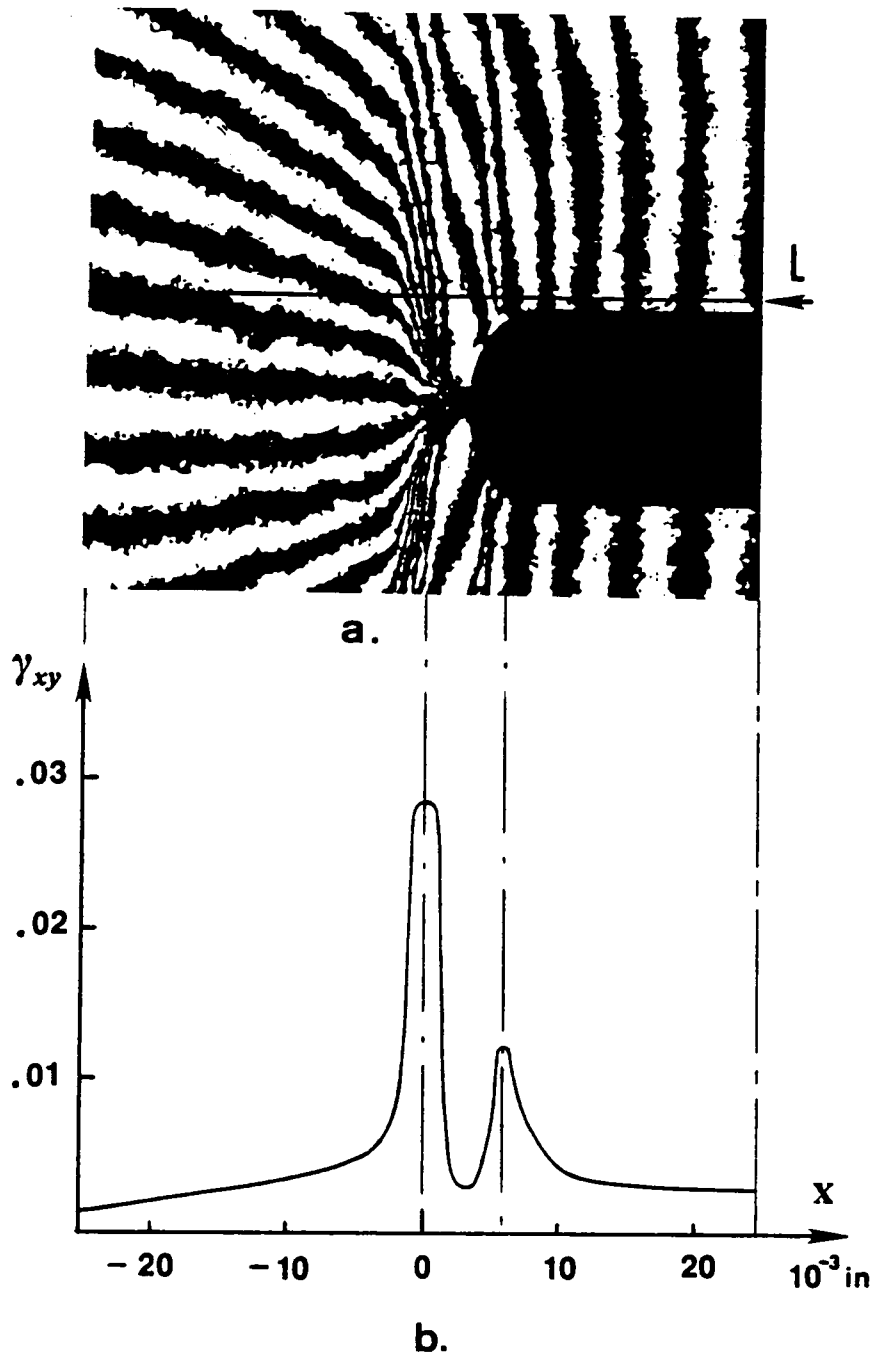

Fig. 1-1. Shear strain measured by moire interferometry, a. Moire interferometry fringe pattern depicting the y-displacement field for a metal-matrix composite specimen with a center slot. b. Shear strain distribution along line L.

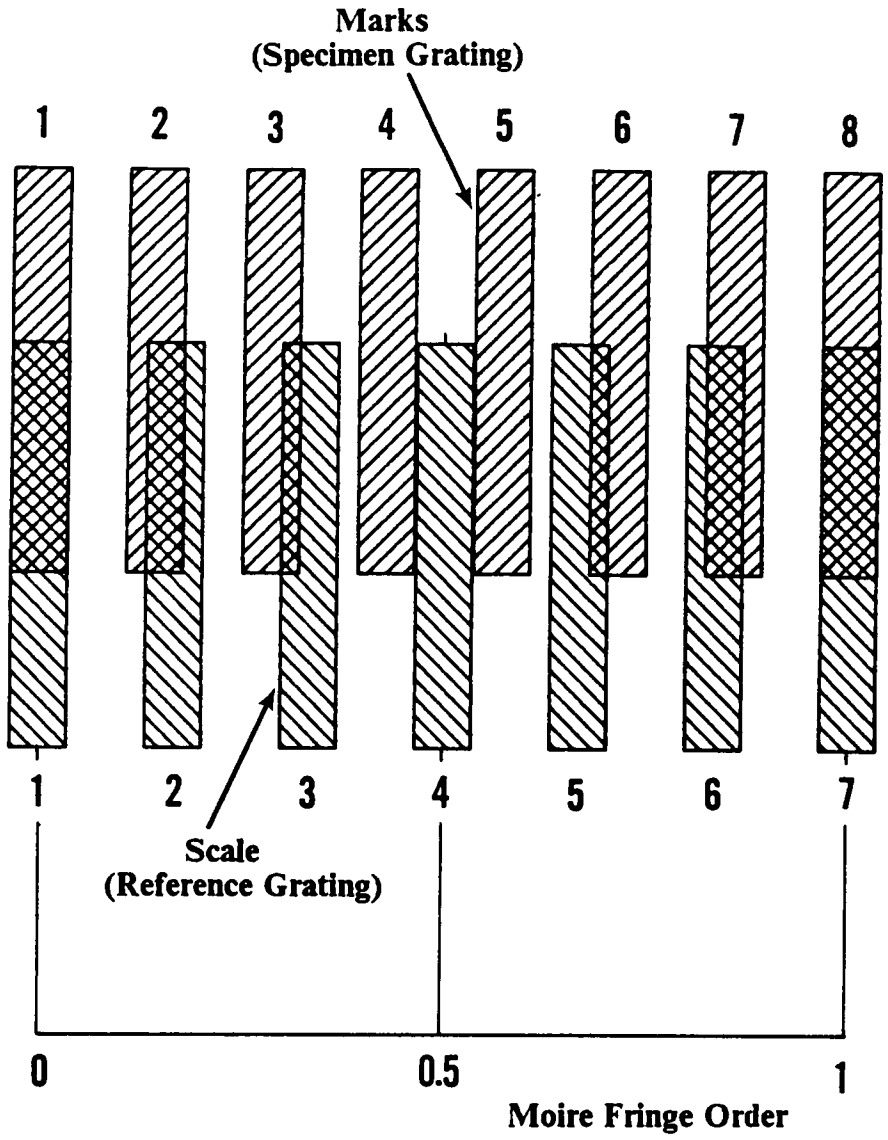

Fig. 1-2. The principle of the geometric moire method

positions of the bars and spaces in the specimen grating are rearranged. The reference grating, which acts as a reference scale, keeps the original position. The fringe pattern represents the differences of the displacement between the two gratings. Moire interferometry is analogous to this, but the scale is a virtual reference grating created by two-beam interference.

Moire interferometry is based on the diffraction theory and the fringe multiplication technique [22,23]. Figure 1-3 shows the optical scheme of a moire interferometer. In this method, a high frequency grating is replicated on the specimen, and it deforms together with the loaded specimen. A virtual grating created by interference of two coherent beams B_1 and B_2 is used as a reference grating and is superimposed on the specimen grating. The specimen and reference gratings interact to form a moire fringe pattern which is photographed with a camera focused on the specimen surface.

The rigorous explanation of moire interferometry utilizes diffraction theory. Two coherent beams B_1 and B_2 illuminate the specimen grating from angles of $+\ \alpha$ and $-\ \alpha$ respectively and are diffracted by the specimen grating (Fig. 1-4). The plus and minus first diffraction orders I_1 and I_2 from the incident beams B_1 and B_2 carry the information of the deformations of the specimen surface. When the specimen is deformed, the angles of the diffraction beams I_1 and I_2 will change according to the frequency change of the specimen grating following the grating equation

$$\sin \theta_m = \sin \alpha + m\lambda f_s \tag{1.1}$$

where θ is the angle of the diffracted beam, m is the diffraction order, λ is the wavelength of the incident light, and f_s is the frequency of the specimen grating. The interference of I_1 and I_2 create a fringe pattern which is a contour map of the displacement on the specimen surface. The frequency of the fringes is determined by the equation of two beam interference in Eq. 1.2.

$$f = \frac{2}{\lambda}\sin\alpha \quad (1)$$

$$U = \frac{1}{f}N_x \qquad V = \frac{1}{f}N_y \quad (2)$$

$$\epsilon_x = \frac{\partial U}{\partial x} = \frac{1}{f}\frac{\partial N_x}{\partial x} \quad (3)$$

$$\epsilon_y = \frac{\partial V}{\partial y} = \frac{1}{f}\frac{\partial N_y}{\partial y} \quad (4)$$

$$\gamma_{xy} = \frac{\partial U}{\partial y} + \frac{\partial V}{\partial x} = \frac{1}{f}\left[\frac{\partial N_x}{\partial y} + \frac{\partial N_y}{\partial x}\right] \quad (5)$$

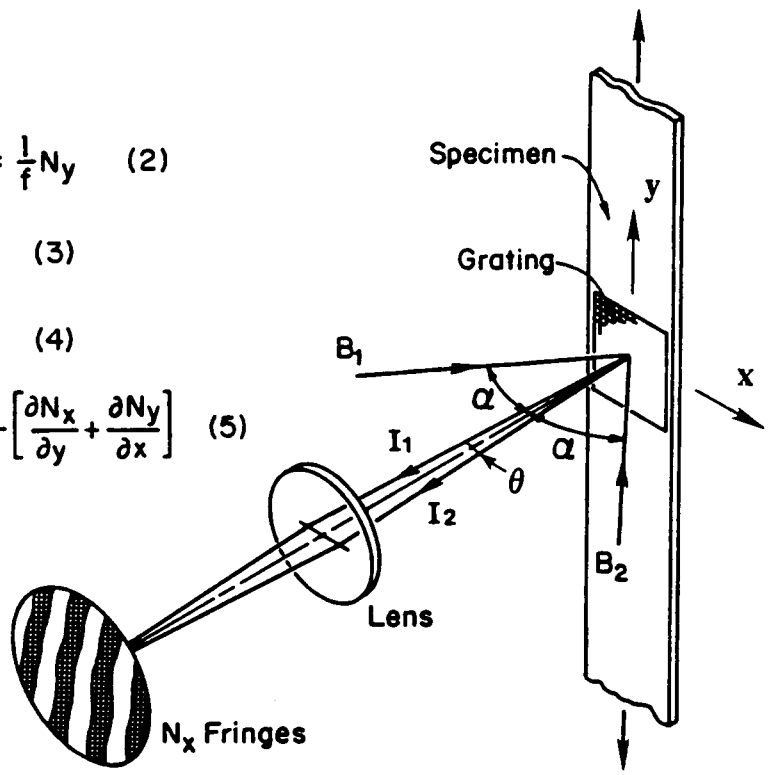

Fig. 1-3. Moire interferometry and relevant equations

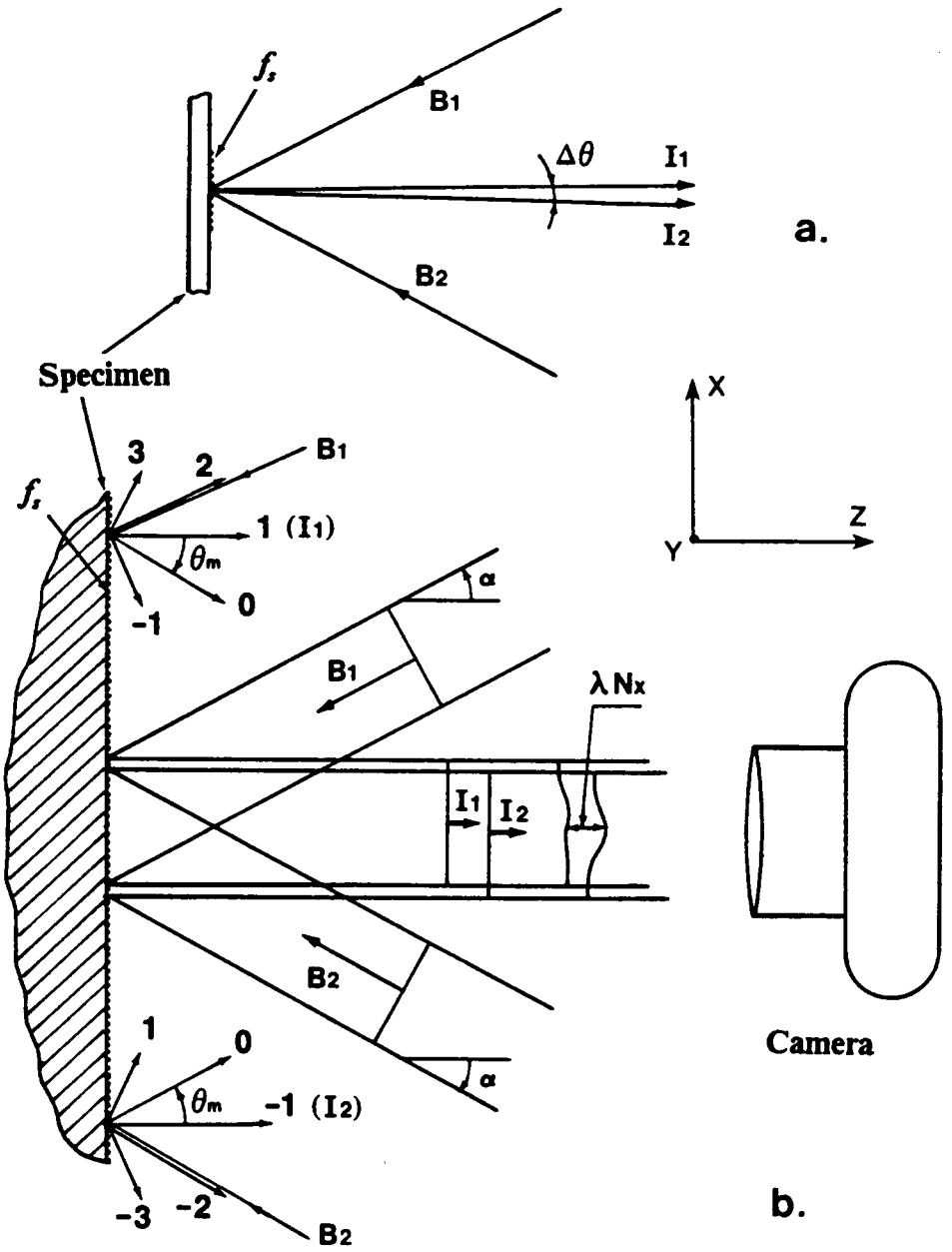

Fig. 1-4. The rigorous explanation of moire interferometry by the diffraction theory. a. Schematic ray diagram of moire interferometry. b. Diffraction beams produced by the specimen grating. The plus and minus first diffraction order I_1 and I_2 from two incidence beams B_1 and B_2 form a fringe pattern on the camera back.

$$F = \frac{2 \sin \Delta\theta}{\lambda} \tag{1.2}$$

where $\Delta\theta$ is the angle between the two diffracted beams I_1 and I_2 , and λ is the wavelength.

From this point of view, it is not necessary to employ the concept of a virtual reference grating, which was presented in the first explanation of moire interferometry by analogy to the geometric moire method. Actually, it does not matter whether the two beams B_1 and B_2 form a virtual grating or not (they do not in certain cases). When the diffracted beams I_1 and I_2 from the specimen grating are mutually coherent, a fringe pattern will be created by the interference of these two beams.[1] A rigorous explanation of moire interferometry does not involve a reference grating [20]. However, the thought of using a virtual reference grating to explain moire interferometry as an analogue of geometric moire is very effective. This thought, proposed by Post, unified moire interferometry and the geometric moire method and created a simple and clear way to explain and understand the principle of moire interferometry [24,25,26]. In the following, the concept of a virtual reference grating is applied frequently in the analysis of moire phenomena and various moire systems.

The fringe pattern presents the magnitude of the displacement in the direction perpendicular to the lines of the reference grating. Each fringe represents a contour curve, and each point on the curve experiences the equal displacement in the defined direction. Usually, two orthogonal displacement fields U and V are recorded by photographing two fringe patterns generated by orthogonal sets of specimen gratings and reference gratings

---

[1] Consider beam B_1 and B_2 in Fig. 1-4, when their polarizations are in the horizontal plane, i.e., perpendicular to the y axis. Then, when $\alpha = 45°$, the two beams are orthogonally polarized, so they cannot interfere to produce a virtual reference grating. Nevertheless, the diffracted beams that reach the camera have parallel polarizations and they interfere to create the moire pattern. The conceptual analysis of moire interferometry by a virtual reference grating is still effective, although sometimes the interference grating does not actually exist.

(Fig. 1-5). Symbols U and V represent displacement components in the x and y directions, respectively. After the fringe orders are assigned by knowledge of boundary conditions, the displacement at any point in the field is determined by

$$U = \frac{N_x}{f} \quad ; \qquad V = \frac{N_y}{f} \tag{1.3}$$

where f is the frequency of the reference grating, N_x is the fringe order at any point in the U displacement field and N_y is the fringe order at the same point in the V displacement field. When the displacement fields are established, the strains can be calculated from the displacement derivatives by the well known small-strain equations:

$$\varepsilon_x = \frac{\partial U}{\partial x} \quad ; \qquad \varepsilon_y = \frac{\partial V}{\partial y} \tag{1.4}$$

$$\gamma_{xy} = \frac{\partial U}{\partial y} + \frac{\partial V}{\partial x} \tag{1.5}$$

1.1.2 Sensitivity and resolution

The sensitivity of an indirect system of measurement is defined as the ratio of the input quantity to the output quantity. In moire interferometry, the input is the displacement ΔU, and the output is the fringe order ΔN. The sensitivity is $\Delta U/\Delta N$ or the displacement per fringe order. If a 2400 lines per millimeter reference grating is used, the sensitivity is 0.417 micrometer displacement per fringe order.

The sensitivity resolution is defined as the smallest true variation of input that can be detected by the system, or the maximum error that could be created by the system. In interferometrical measurements, the sensitivity resolution can be made very high by

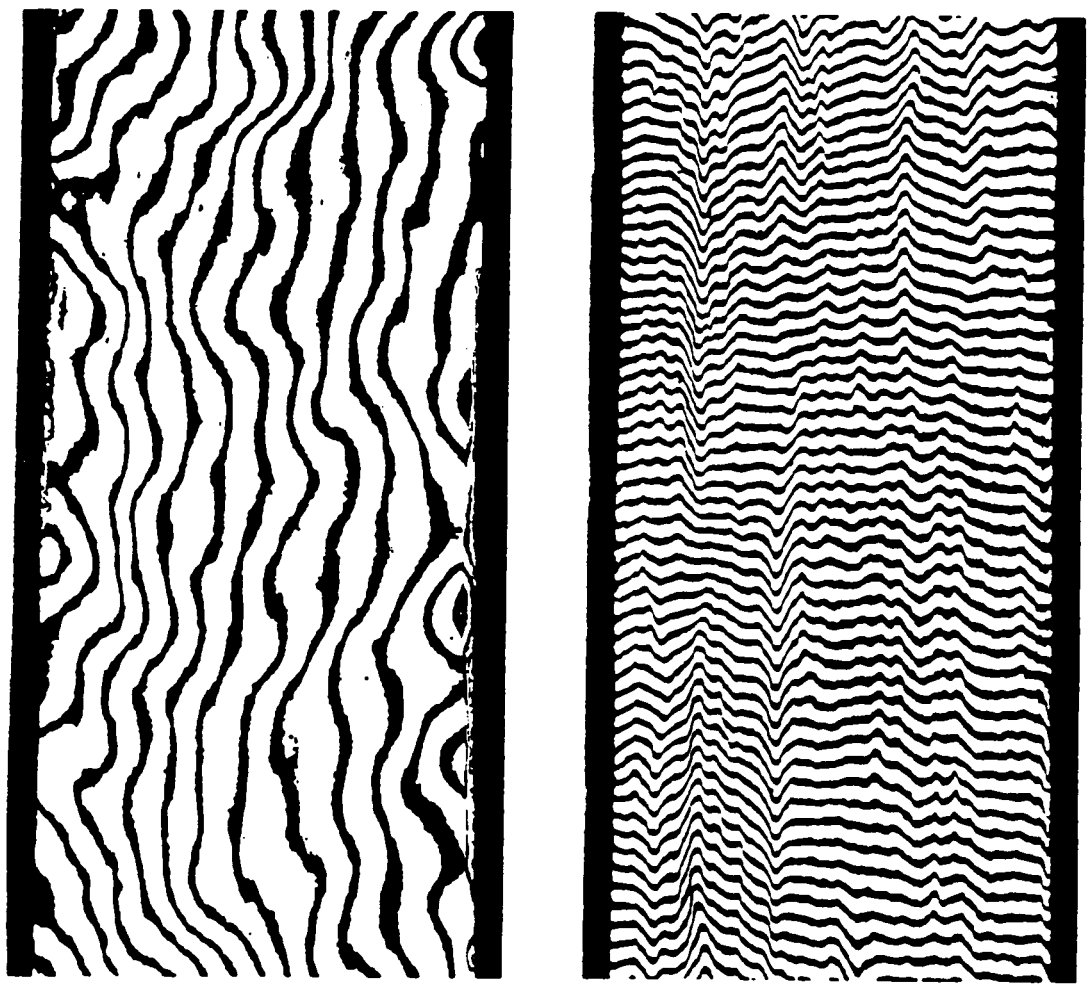

Fig. 1-5. Moire fringe patterns are contour maps of the U and V components of displacement. The pictures were obtained from a test of a graphite/epoxy woven composite specimen, loaded in compression along its y axis [15].

interpolation between fringe centers through knowledge of the fringe order vs. intensity relationship. In addition to the need for special procedures and equipment, interpolation of fringe intensity is subject to various limitations. In the present work, interpolation of fringe intensities between maximi and minimi is not used. Instead, the centerlines of both dark and bright fringes are used as the accurate data points (Fig. 1-6). Accordingly, the sensitivity resolution is about 0.2 micrometer displacement or the maximum error is 0.2 micrometer displacement in moire interferometry, if the reference grating has 2400 lines per mm [20]. Further interpolation without using special procedure is not always accurate. In the cases where strain variations are dramatic, the important information of strain concentrations could be missed because of insufficient sensitivity resolution. The way to circumvent this problem is to get more accurate data points between the centerlines of two neighboring fringe. In moire interferometry the number of data points can be increased by introducing carrier fringes. This technique will be discussed in Chp. 2.

More data points mean denser fringes, and in order to interpret a dense fringe pattern, an image recording system of high spatial resolution is required.

Spatial resolution is determined by the resolution of the optical system that records the fringe patterns. High spatial resolution enables moire interferometry to measure the high displacement variations in a very small zone. This is extremely valuable in the study of composite materials because investigators are interested in the deformations of the plies, fibers and the boundaries of fibers and matrix. In the corresponding small zones, several data points have to be obtained if the displacement distributions are to be determined. The spatial resolution is restricted by the image recording system. If the camera and the film have very good spatial resolution, the finer structures can be investigated. Spatial resolution of one micrometer is the present situation in the VPI & SU photomechanics laboratory.

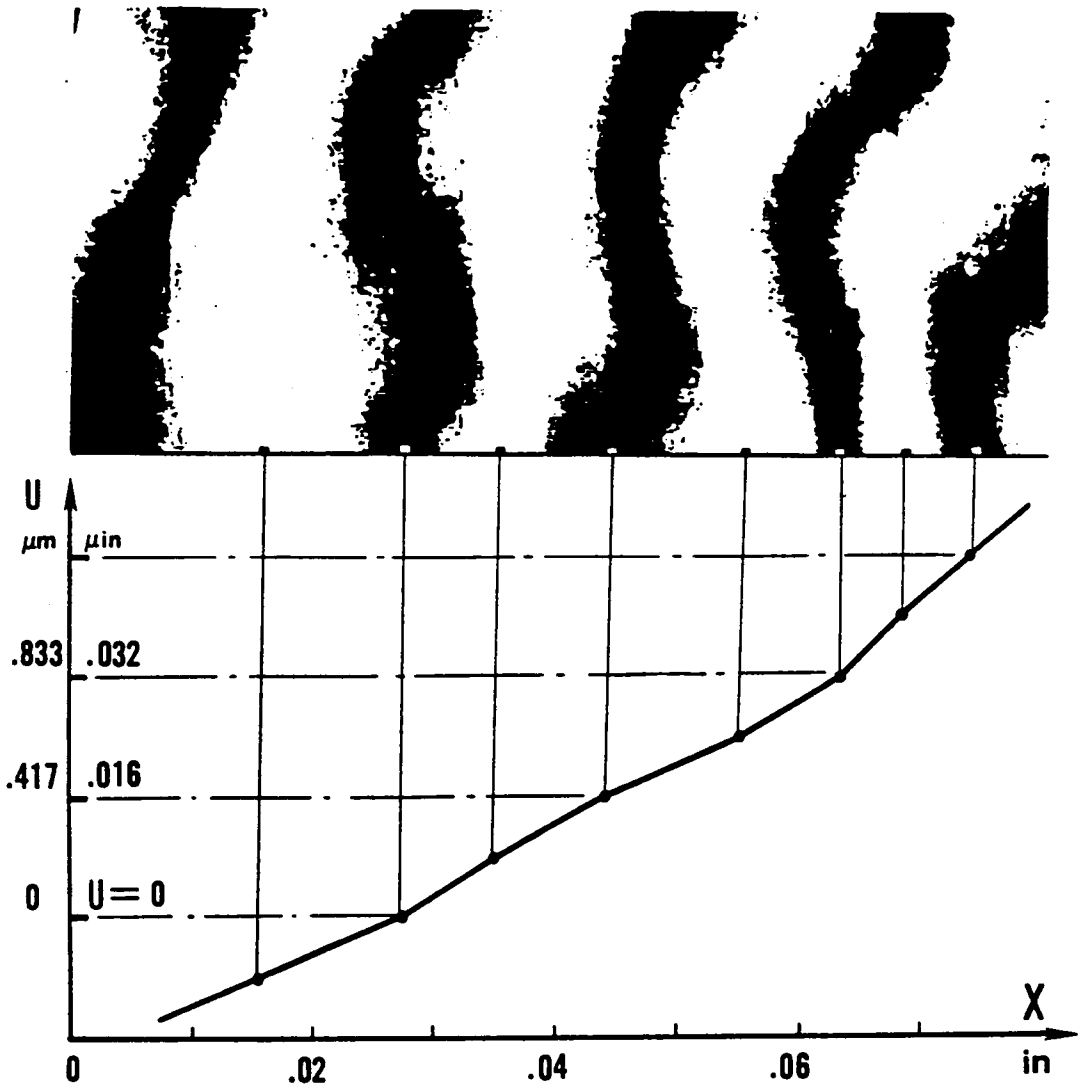

Fig. 1-6. The sensitivity resolution is the displacement represented by half fringe order, The center lines of dark and bright fringes are used as the accurate data points.

1.1.3 Range of measurement

Generally, a system has a narrower range of measurement if its sensitivity is high. Moire interferometry, however, has a comparatively wide range of measurement although its sensitivity is very high.

Figure 1-7 shows a test result from a woven composite specimen under compression [27]. The large variation of the shear strains from zero to 5.6 percent strain was measured from the same fringe pattern. The wide range of measurement enables moire interferometry to record large and small strains at the same time and from the same fringe pattern with very high sensitivity. This is one of the unique properties of the moire technique.

The lower limit of measurement range is restricted by the sensitivity resolution. [2] The upper limit is restricted by the spatial resolution. To increase the range of measurement, both resolutions have to be improved. In the VPI&SU photomechanics laboratory, the sensitivity resolution of 0.2 micrometer displacement is obtained (without using any special procedure to interpolate fringe intensity), such that for a testing area that has one dimension of one inch , a strain as small as 8 microstrain can be resolved by this sensitivity resolution.[3] Spatial resolution of 1 micrometer is achieved, such that on a testing area, if the fringe density reaches to the resolving limit of the spatial resolution, the corresponding strain measured is 0.42, or 42% strain[4] which is the upper limit of the measurement.

---

[2] See the definitions of sensitivity resolution in Section 1.1.2.

[3] Assuming that the testing area has the width of one inch, the smallest strain that can be measured is the sensitivity resolution divided by the width of the testing area, which is $0.2\mu m/25mm = 8$ microstrain

[4] Assuming that the fringe pitch is equal to the limit of spatial resolution ($1\mu m$), the maximum strain measured is: $\text{strain} = \frac{1}{f}\frac{\Delta N}{\Delta x} = \frac{1}{2400/mm}\frac{1}{1\mu m} = 0.42$ strain

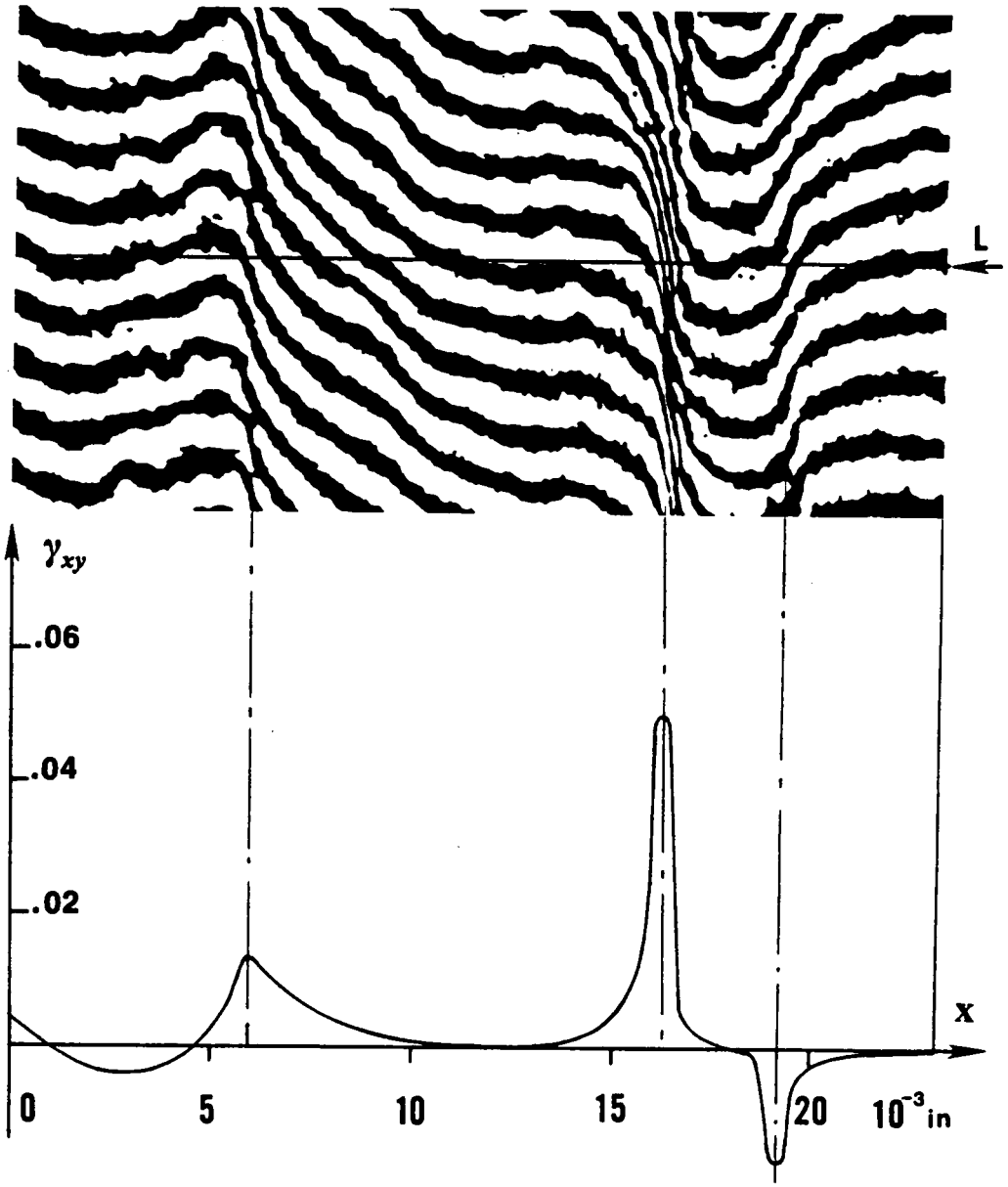

Fig. 1-7. The range of measurement, strain variation, from zero strain to 0.056 strain, is recorded in the same fringe pattern. The derivative $\frac{\partial V}{\partial x}$ is obtained from this pattern of the V field. In the corresponding U field, the derivative $\frac{\partial U}{\partial y}$ is negligibly small.

1.1.4 Fringe ordering

Moire fringes are defined as isothetic lines in reference [28], which means that all the points on a fringe line have the same displacement component; it is known also as a contour line of constant displacement component. The information presented by a fringe pattern is the magnitude of relative displacement in the direction defined by the perpendicular to the direction of the reference grating lines. A displacement field can not be defined from fringe patterns unless fringe orders are known. The process of determining fringe orders is called fringe ordering.

In moire interferometry, the in-plane displacements are measured. To fully define the displacement at a point (x,y) in a plane displacement field, one needs to know both magnitudes and signs of displacements $U(x,y)$ and $V(x,y)$ which can be expressed as

$$\begin{aligned} U(x,y) &= U_o(x_o,y_o) + U_r(x,\ y) \\ V(x,y) &= V_o(x_o,y_o) + V_r(x,\ y) \end{aligned} \tag{1.6}$$

where U_r, V_r are displacements of point (x,y) in x and y direction relative to the reference point (x_o,y_o), which has the displacement of U_o and V_o. The rigid body movements represented by the constants U_o and V_o have no influence on the deformations, and they can be neglected. Accordingly, an arbitrary point can be chosen to set $U_o = V_o = 0$, so that $U = U_r$, $V = V_r$. In most of the experiments, the U and V displacement fields are photographed simultaneously and the two fringe patterns obtained contain only the information of the magnitudes of U and V displacements. To determine the relative displacement field, the signs of U and V or the orders of fringes have to be determined from the boundary conditions. Usually, the boundary conditions can be obtained from the loading conditions and the mechanical properties of the testing material. For instance, if a specimen is loaded in a longitudinal direction then the fringe order can be assigned

because in this direction, the displacement is defined by the sign of the load. Generally, the transverse displacement can also be determined by the Poisson effect if the material is isotropic. If the material is anisotropic or the deformation measured is caused by external conditions other than mechanical load, it may be difficult or impossible to assign the fringe orders by the fringe patterns themselves.

For a given pair of moire fringe patterns of U and V displacement, if no boundary condition is applied, there are four combinations of signs that are possible for the displacements at an arbitrary point A. Figure 1-8a shows these four possibilities which are (u,v), (u,-v), (-u,v) and (-u,-v). After one boundary condition is applied, for example $u > 0$, the possibilities reduce to two which are (u,v) and (u,-v). One more boundary condition is necessary to determine the displacement field, e.g. if $v < 0$, is applied, the solution must be (u,-v). The conclusion is that if two fringe patterns are available, two boundary conditions are necessary to determine the unique solution.

At any point of a plane displacement field, displacements can be expressed by any two of the orthogonal components which have the same resultant displacements. Therefore, if the third fringe pattern is photographed and the magnitude of one more displacement field is known in a direction different from the first two, the resultant displacement can be expressed by this component and a component perpendicular to it. As shown in Fig. 1-8b, if the displacement component in 45 deg is known, by combining the -45 deg component, one should get the same resultant displacement as combining 0 and 90 deg components. In the case of knowing the magnitude of the third component, only one boundary condition is enough to determine the displacement field. For instance (Fig. 1-8b), if magnitudes of U and V are fixed and one boundary condition is given as $u > 0$, the possibilities of the real displacement at point A are (u,v) and (u,-v). By knowing the magnitude of the displacement component in 45 deg. direction, the displacement can be determined as (u,v). Because when the magnitude in 45 deg. is fixed,

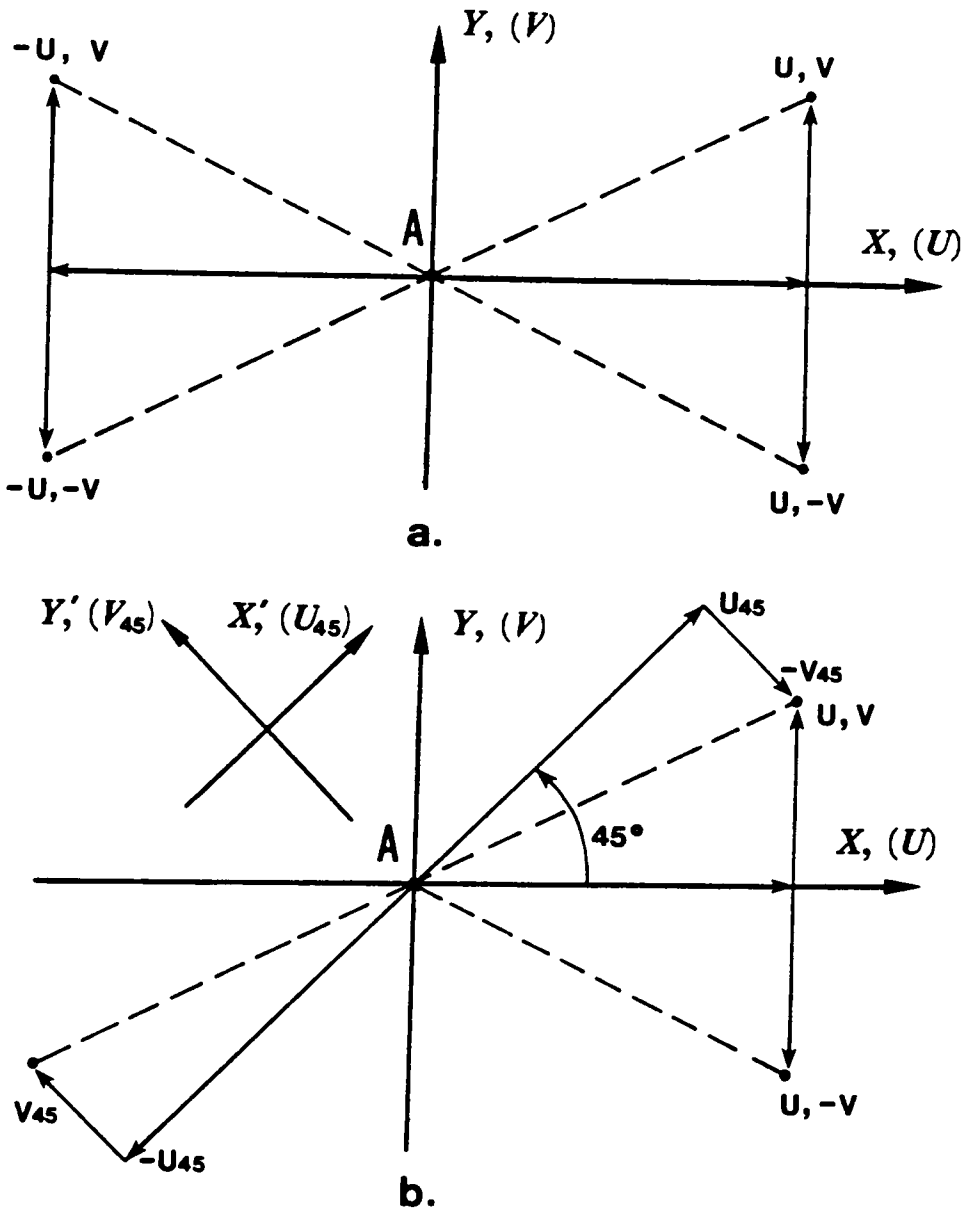

Fig. 1-8. Displacement components and boundary conditions. a. If only the magnitudes of U and V displacements are known, there are four possibilities for the displacement at an arbitrary point A. Two boundary conditions have to be applied to determine the true displacement, e.g. $u > 0$ and $v < 0$. b. If the magnitude of displacement component is known in third direction, e.g. U_{45}, the boundary condition can be reduced to only one, e.g. $u > 0$.

there is only one choice of resultant displacements satisfying both groups of orthogonal components. In practice, the 45 deg. fringe pattern of displacement can be obtained very easily by using the technique presented in reference [29]. Further increasing of fringe patterns and knowing more components of displacements is not helpful in eliminating the boundary conditions as shown in Fig. 1-8b. For all circumstances, at least one boundary condition is required to give fringe patterns the physical meaning and link the fringes to the displacements. Fortunately, in most experiments, when there is an applied mechanical load, it is easy to obtain at least one boundary conditions by using the loading condition. If the 45 deg. fringe pattern is photographed to give the magnitude of displacement in the third direction, the displacement field can be determined. For the cases that there is no boundary condition available, experimental methods have to be applied to determine fringe orders [28,30].

When the signs of displacements are obtained, fringe orders can be assigned and the sign of the fringe gradient can be determined. Since U_0 and V_0 are arbitrary, the sign and the number which are used for fringe ordering are arbitrary. The sign of the fringe gradient is important because it is used to calculate displacements and strains.

Usually it is sufficient to determine the sign of the fringe gradient only at one point in the field. If the fringes can be continuously ordered, or there is no discontinuity through the whole field, the whole field displacement and strain can be determined.

1.2 Limitations and Objectives

As mentioned before, moire interferometry has very high sensitivity and resolutions

compared to other electric and optical methods of displacement measurement.[5] It has been used successfully to measure macromechanical properties of many kinds of materials. Especially for composite materials, moire interferometry can be used to investigate the displacement distributions on the surfaces of specimens with various geometries and the displacement variations created by their anisotropic properties.

Moire interferometry has the potential to be used for micromechanics measurements. Some experiments have been performed to investigate the micromechanical properties of composite materials and the results are very encouraging [13,14,15]. However, when measuring strain variations in the micromechanics region, sometimes very localized strain concentrations are undetected because of the lack of resolution of fringe gradients. In chapter 2 of the dissertation, a carrier fringe technique is developed to increase the resolution of fringe gradients, and experimental verifications are presented.

Because of the high sensitivity, moire interferometry is strongly restricted by the environment. A tiny vibration could wash out the fringe pattern entirely. So far, most of the experiments and tests have been performed in the optical laboratory environment and on optical tables. This situation very much limited the applications of moire interferometry and usually made the technique quite expensive. Especially in composite material testing, because of the high strength and stiffness, high loads are required to investigate deformations and failures. The optical laboratory usually cannot satisfy the testing requirements. It is crucial to create a new moire system that can tolerate the environment sufficiently to move the moire technique into a material testing laboratory or even a mechanical shop environment.

---

[5] Speckle interferometry has the same sensitivity and resolution. However, the fringe contrast and the range of measurement are inferior.

In chapter 3, new moire systems which are relatively insensitive to vibrations are introduced. The designs and analyses are presented. As demonstrations, the experiments are performed using these interferometers on a mechanical testing machine to verify the properties.

2.0 Increasing Resolution of Fringe Gradients by Carrier Fringe Technique

2.1 Introduction

A fringe pattern gives the information of strains on specimens by the fringe gradients. As shown in the equations in Fig. 1-3,

$$\varepsilon_x = \frac{1}{f}\frac{\partial N_x}{\partial x} \quad ; \quad \varepsilon_y = \frac{1}{f}\frac{\partial N_y}{\partial y}$$

$$\gamma_{xy} = \frac{1}{f}\left(\frac{\partial N_x}{\partial y} + \frac{\partial N_y}{\partial x}\right)$$

the strains are calculated by the partial derivatives which are presented by fringe gradients in fringe patterns. When fringe gradients are extracted from a fringe pattern, the center lines of fringes are used as the data points. As shown in Fig. 2-1, if the center lines of black and white fringes are used as the data points, there is only one data point

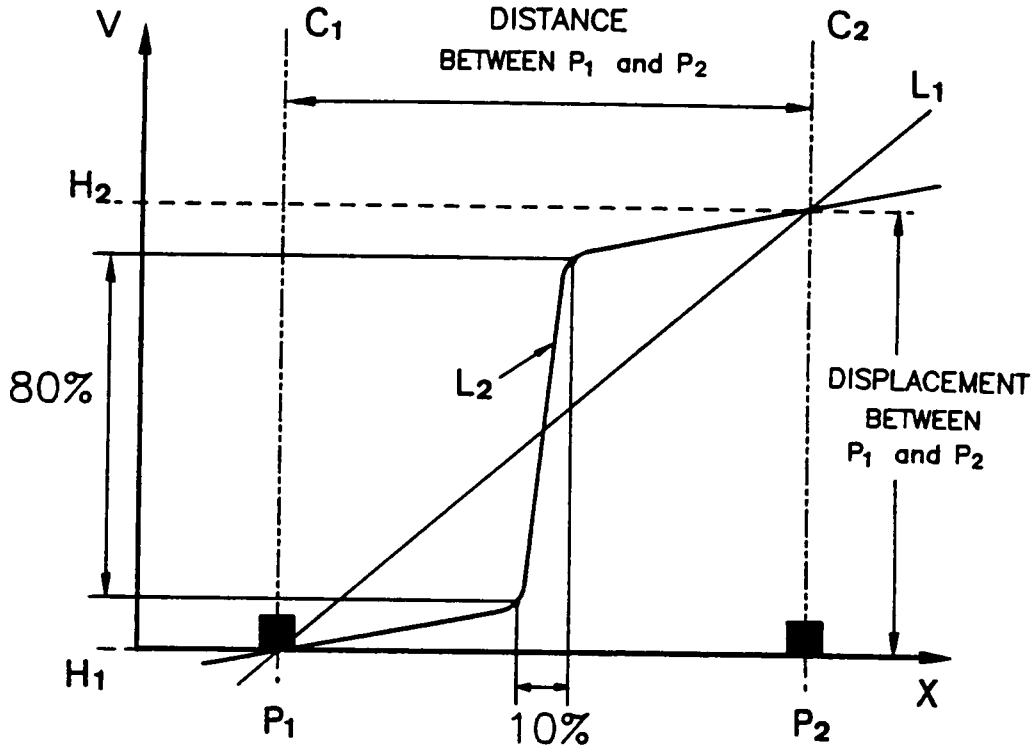

P1 , P2 : POSITIONS OF TWO NEIGHBORING FRINGES
C1 , C2 : CENTER LINES OF TWO NEIGHBORING FRINGES
L1 : LINEAR APPROXIMATION OF DISPLACEMENT
L2 : REAL DISTRIBUTION OF DISPLACEMENT

Fig.2-1. The distributions of displacement between two neighboring fringes

between two black fringes which gives the displacement of one fringe order increase. One can not get an accurate displacement distribution and resolve the strain variation between the neighboring two data points unless a sophisticated grey level technique is used, and this is not practical in many circumstances. Usually, a linear interpolation is applied to approximate the variation. Sometimes, it is found that this approximation is far from the truth. As shown in Fig. 2-1, the displacement curve between two fringes P_1 and P_2 could be any curve bounded by two lines H_1 and H_2 which give the displacement of one fringe order increase. If the true displacement distribution is curve L_2, the maximum strain (strain concentration) involved is eight times higher than the average strain presented by curve L_1 which is the linear approximation. In composite material testing, the displacement usually varies dramatically at the boundary of a fiber and matrix and the boundary between plies. The linear approximation would often miss some important information. By introducing carrier fringes, the data points between the two neighboring fringes can be significantly increased which will help resolve the fringe gradients and the strain distributions.

2.2 Carrier Fringes

In geometric moire, the carrier fringes have been called *mismatch fringes* [31]. They are introduced by changing the frequency or the orientation of the reference grating. In the case of moire interferometry, a very large number of carrier fringes (or *mismatchfringes*) is sometimes introduced, even many times the number of load-induced fringes [32]. In such cases, a high-frequency pattern of uniformly spaced carrier fringes is modulated by the load-induced changes of fringe orders. The analogy to carrier frequencies in communications technology is strong, and similar terminology is adopted.

As used here, the terms of *carrier fringes* and *carrier patterns* represent any carrier fringe frequency: high or low, positive or negative. These carrier fringes can increase or decrease the frequency of load-induced fringes. The term *mismatch* does not apply consistently to moire interferometry. The word implies a difference in frequency and orientation of specimen and reference gratings. However, moire interferometry can operate when there is no reference grating at all, neither a real reference grating nor a virtual reference grating,[6] but carrier fringes can be produced in such a case. The term *carrier* is meaningful even when *mismatch* is not, so *carrier fringes* will be the terminology favored here.

In moire interferometry, the direction and the frequency of the reference grating is changed by adjusting the incident beam B_1 or B_2 (Fig. 1-3). Experimentally, this is usually done by a thumbscrew adjustment of one optical element, e.g., a mirror that directs light into B_1. A carrier pattern of extension, composed of fringes parallel to the lines of the specimen grating, is obtained by a small change of the magnitude of angle 2α . A carrier pattern of rotation, composed of fringes essentially perpendicular to the lines of the specimen grating, is obtained by a small inclination of the plane that contains B_1 or B_2 with respect to the x-z plane or by a small rigid body rotation of the specimen grating.

In moire interferometry, carrier fringes can be used for various purposes. The technique is very important and effective in strain and displacement analysis. In composite material testing, it is especially powerful for investigating strain concentrations and strain variations [32].

---

[6] see chapter 1 for the explanation

2.3 Fringes and Fringe Vectors

There are two ways to obtain fringes. One is to deform the specimen grating by external loads or other means, and the other one is to change the reference grating. The first one introduces load-induced fringes, and the second one introduces carrier fringes.

The fringe gradient has vector properties as illustrated in Fig. 2-2. At an arbitrary point, a fringe vector F is defined such that it is perpendicular to the tangent to the fringe at that point and has a direction toward the direction of increasing fringe orders. Its magnitude is proportional to the gradient of the fringes along the defined direction. All the rules of vector calculation can be applied to the fringe vector. A fringe vector can be decomposed into two orthogonal components F_x, F_y which are independent of each other and related by the equation

$$F_y = F_x \tan \phi \tag{2.1}$$

where F_x, F_y represent the fringe gradients $\partial N/\partial x$ and $\partial N/\partial y$ respectively, and $\tan \phi$ is the slope of the fringe vector, or the reciprocal of the slope of the fringe.

When a carrier pattern is introduced, the resultant fringe vector is equal to the vector sum of the load-induced fringe vector and the fringe vector of the carrier pattern. At any point of the fringe pattern

$$F_x = F_{lx} + F_{cx} \quad ; \quad F_y = F_{ly} + F_{cy} \tag{2.2}$$

where subscript l represents the load-induced fringes and the subscript c represents the carrier fringes. Thus, Eq. 2.1 can be written as

$$F_{ly} + F_{cy} = (F_{lx} + F_{cx}) \tan \phi \tag{2.3}$$

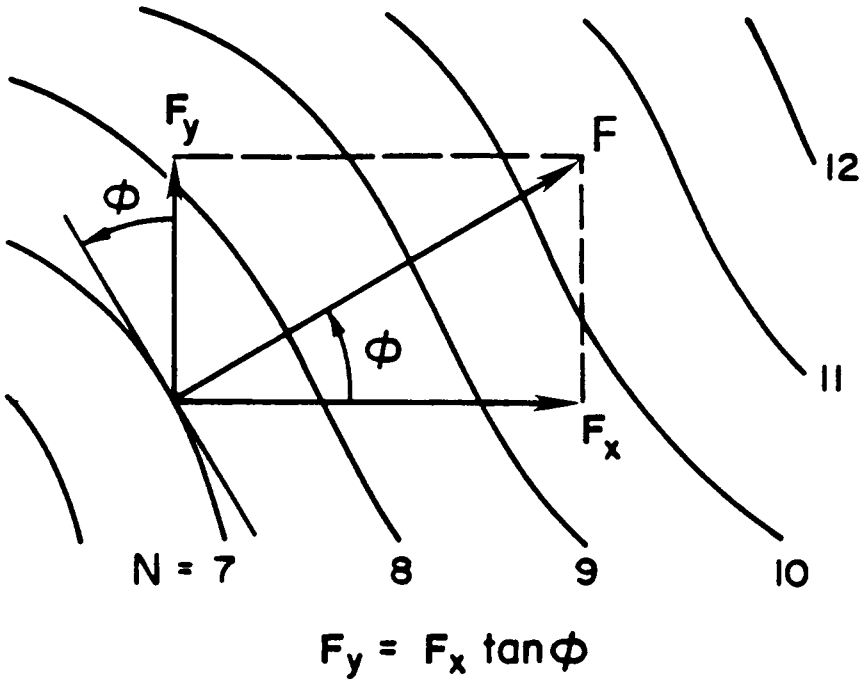

Fig.2-2. Fringe azimuth and fringe vectors

In terms of the fringe vector and its components, the displacement derivatives can be written as: for the U (x direction) displacement field,

$$\frac{\partial U}{\partial x} = \frac{1}{f} F_{lx} \quad ; \qquad \frac{\partial U}{\partial y} = \frac{1}{f} F_{ly} \tag{2.4}$$

for the V (y direction) displacement field,

$$\frac{\partial V}{\partial y} = \frac{1}{f} F_{ly} \quad ; \qquad \frac{\partial V}{\partial x} = \frac{1}{f} F_{lx} \tag{2.5}$$

and the strains can be determined by Eqs. 1.4 and 1.5.

Notice that carrier fringes are not required, in principle, to determine strains. Carrier fringes can be used , however, to transform the pattern to one from which the load-induced gradients can be extracted with enhanced resolution and precision.

2.4 Carrier Fringes of Rotation

It is necessary to clarify the special properties of carrier fringes of rotation before the application. Carrier fringes of rotation are oriented perpendicular to the bisectors of the initial specimen grating lines and the reference grating lines (Fig. 2-3). Consequently, the carrier fringe vector has two components which are functions of γ , [7]

$$F_c = \gamma f \quad ; \qquad F_e = -\frac{\gamma^2 f}{2} \tag{2.6}$$

where γ is the angle between the initial specimen grating lines and the reference grating lines (Usually to introduce sufficient carrier pattern of rotation, γ is less than 0.1 rad.).

---

[7] Refer to Appendix A.

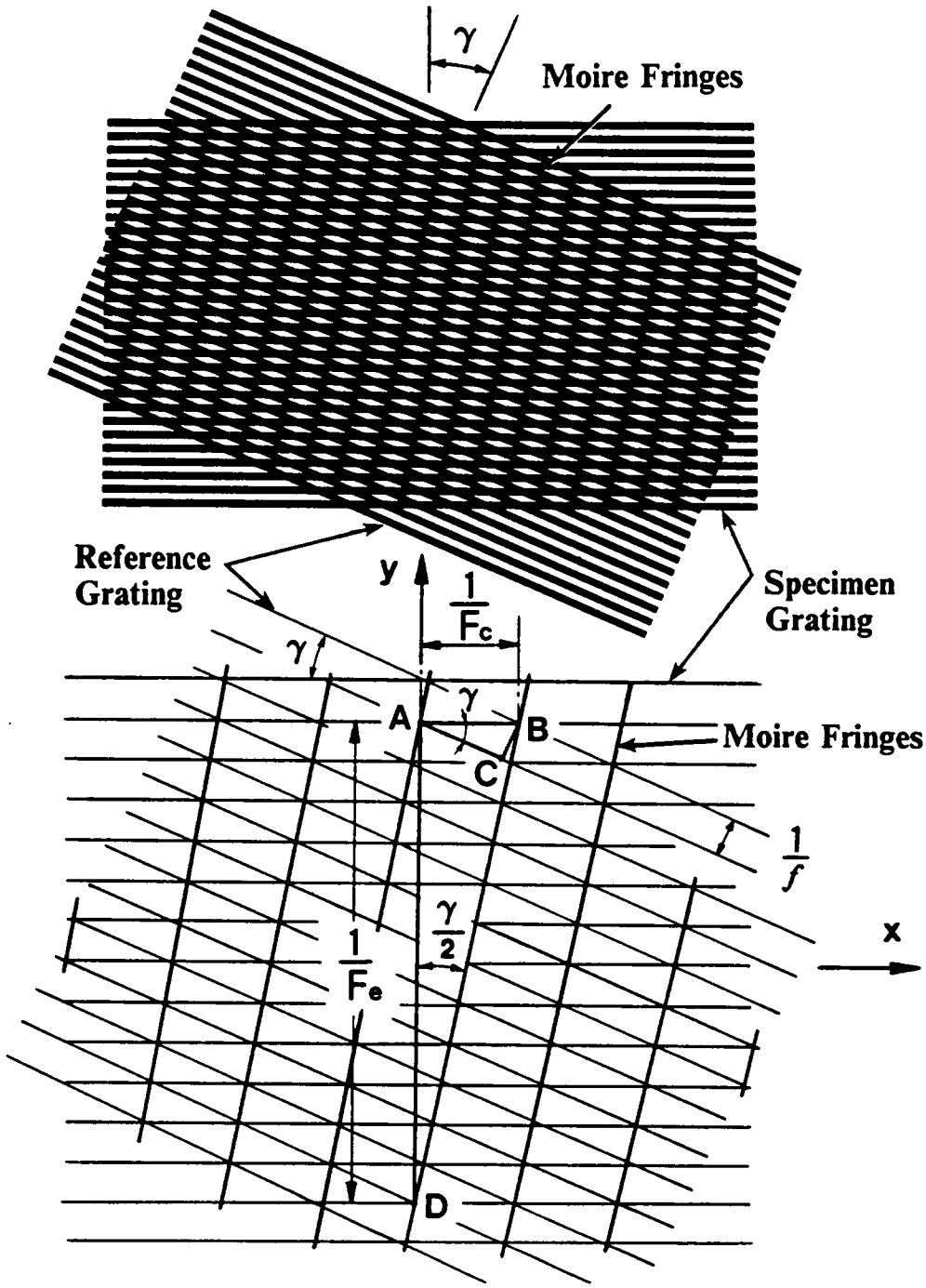

Fig. 2-3. The carrier fringes of rotation. a. The carrier fringes of rotation introduced by the relative rotation of angle γ between the specimen grating and the reference grating. b. The gradient of carrier fringes of rotation has two components, the desired carrier fringes F_c and the extraneous fringes F_e.

F_c is the desired component of the carrier fringe vector of rotation and it lies parallel to the specimen grating lines. F_e is the extraneous component of the carrier fringe vector and it lies perpendicular to F_c. For a fixed coordinate system aligned with the initial orientation of the specimen grating lines, the extraneous component F_e is always negative. It is an apparent uniform compressive strain on the specimen surface. In practice, angle γ is usually very small and the extraneous component is usually negligible. For example, if F_c is 10 fringes/mm and if the frequency of reference grating f is 2400 lines/mm, it is found that ϕ is 0.004 radians, and F_e is 0.02 fringes/mm. The apparent extraneous strain ε_e is -9 $\mu m/m$. Thus, the effects are very small. When a very strong carrier pattern of rotation is used in some special cases, however, the extraneous effects might not be negligible. In such cases, corrections can be applied by using Eqs. 2.2 and 2.6.

The carrier pattern of rotation can be produced in two ways:

1. by rigid-body rotation of either the specimen grating or the reference grating relative to the other.

2. by adjustment of beam B_1 (and/or B_2) illustrated in Fig. 1-3.

Equations 2.6 apply directly to case (1). For case (2), one must consider the great variety of optical systems that can be used to produce beams B_1 and B_2 [20]. No common analysis can be given for the carrier fringes in terms of the adjustments of the mirrors or optical elements. Instead, means to maintain F_e within acceptable limits must be considered on an individual basis.

2.5 The Carrier Fringe Method

The pure carrier fringes, extension or rotation, have constant slopes and frequencies, just as the fringes created by uniform normal or shear strains. When a carrier pattern is added to a load-induced fringe pattern, the fringe slope and frequency at any point is modified by the local strains [32]. If the fringe vector is used to express the fringe gradient (Fig. 2-2), the slope of the fringe vector, which is the reciprocal of the fringe slope, is

$$\tan \phi = \frac{F_y}{F_x} \tag{2.7}$$

where F_x and F_y are two components of the fringe vector F at an arbitrary point of the displacement field. As mentioned before, they represent the fringe gradients in x and y directions respectively, and can be further defined as the sums of fringe gradients introduced by carrier fringes and load-induced fringes (Eq. 2.2). From Eq. 2.7, if one of the components is known, the other one can be determined by the fringe slope. For example, if F_x is known, then $F_y = F_x \tan \phi$. The question of resolving fringe frequencies F_y is transformed to that of resolving the fringe slopes $\tan \phi$. The fringe slope is a continuous function along a fringe. In principle, it can be measured at any point, not only along the contours of integral or half fringes but also along intermediate contours of constant grey level. It can be measured at any point. Thus, the resolution of fringe gradients becomes theoretically unlimited. In practice, known carrier fringes are introduced to modulate the slopes of load-induced fringes. As shown in Eq. 2.3, the slopes of fringes are controlled by the four quantities, F_{cx}, F_{cy}, F_{lx} and F_{ly}. F_{lx} and F_{ly} are determined by the external load. If F_{cx} and F_{cy} are properly chosen, the load-induced fringes can be modulated into any frequency and direction. The resolution of fringe gradients

can be significantly increased by analyzing the resultant fringes. Since the fringe gradients represent the strains , the resolution increase provides more details of strain distributions.

2.6 Experimental Demonstrations

Fiber reinforced composite laminates consist of two elements, the fibers and the matrix. The fibers usually are much stronger than the matrix and the properties of the composite depend largely on the arrangement of the fibers. For example, when the fiber direction varies from ply to ply, the engineering coefficients are different. In isotopic and homogeneous materials, the engineering coefficients are the same everywhere, but in composite materials, the property changes from layer to layer and the overall laminate property depends upon the arrangement of the layers. In a graphite/epoxy composite, the thickness of a ply is usually about 125 micrometers. For most other measurement techniques, the resolution is not high enough to resolve the displacement variations in a single ply and at the boundaries of plies.

2.6.1 The shear properties of graphite/epoxy composites

Figure 2-4 shows a rail-shear test for determination of interlaminar deformations of a graphite/epoxy specimen with a [90/90/0]n stacking sequence. For analyzing the shear strain, the component $\frac{\partial V}{\partial x}$ is required and the fringe vector F_{I_x} can be measured from the load-induced fringes of Fig. 2-4a. The shear strain distribution along a horizontal line is determined by this procedure and depicted in Fig. 2-4b. Because the specimen is fabricated with successive plies of 90 deg and 0 deg fiber orientations, the

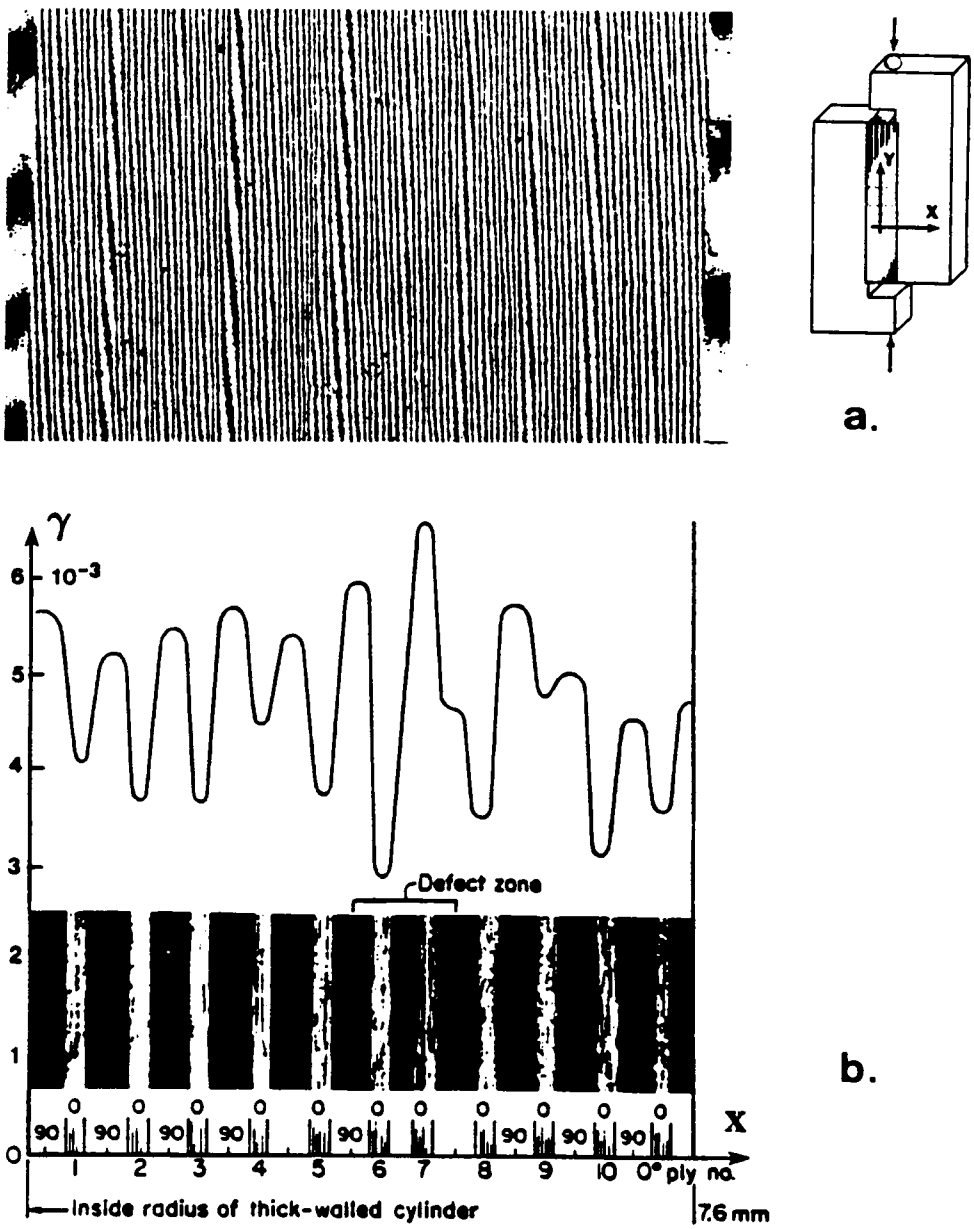

Fig.2-4. Interlaminar shear test of [90/90/0]n graphite/epoxy composite specimen, a. the load-induced fringes of V displacement field, b. the shear strain distribution along a horizontal line across the specimen. Since $\partial U / \partial y = 0$ along this line, the shear strain the data is extracted directly from pattern (a). The insert at the bottom is a photograph showing the ply sequence.

shear strains vary from ply to ply. In certain plies, the deformations are represented by only one fringe. It is impossible to measure the true gradient by only one fringe (unless a sophisticated grey-level technique with very high spatial resolution is applied).

By introducing a carrier pattern of extension F_{cy}, the fringe pattern is transformed to that of Fig. 2-5a. The fringe vector F_{lx} can be calculated by Eq. 2.3 as $F_{lx} = F_y / \tan\phi$, where $F_y = F_{ly} + F_{cy}$. F_y is easily determined in any region from Fig. 2-5a by measuring the vertical (y) distance between fringes. At any point in the pattern, ϕ is determined by the angle of the fringe normal at that point. Since the carrier pattern doesn't affect the fringe vector in the x direction, F_{lx} still represents the required gradients $\frac{\partial V}{\partial x}$. Now, the gradients are revealed at every point in the field, because the fringe angle (and F_y) can be determined at any point. Gradients $\frac{\partial V}{\partial x}$ that could not be recognized from Fig. 2-4b can be calculated with high fidelity from Fig. 2-5a. The shear strain distribution along the same horizontal line is depicted in Fig. 2-5b. It differs from the shear strain distribution extracted directly from the load-induced fringe pattern (Fig. 2-4b). Without the carrier fringes, high strain concentrations were missed because of insufficient resolution. Figure 2-5b offers much more detailed information. The variations in shear strains show that the 0 deg plies have higher shear stiffness than the 90 deg plies and also that high shear strain concentrations appear at the resin-rich zones where the material is most compliant.

As a practical matter, the method is implemented best when ϕ is approximately 45 deg. Detailed normal and shear strain distributions are presented in Ref. [12] for this specimen.

Figure 2-6 shows another example of discovering shear properties by introducing carrier fringes. The specimen is a 48 ply quasi-isotropic beam of graphite-PEEK in a five-point bending test [13]. Figure 2-6b is the fringe pattern of the load-induced U displacement field. The pattern is complicated and it is difficult to assign fringe orders in

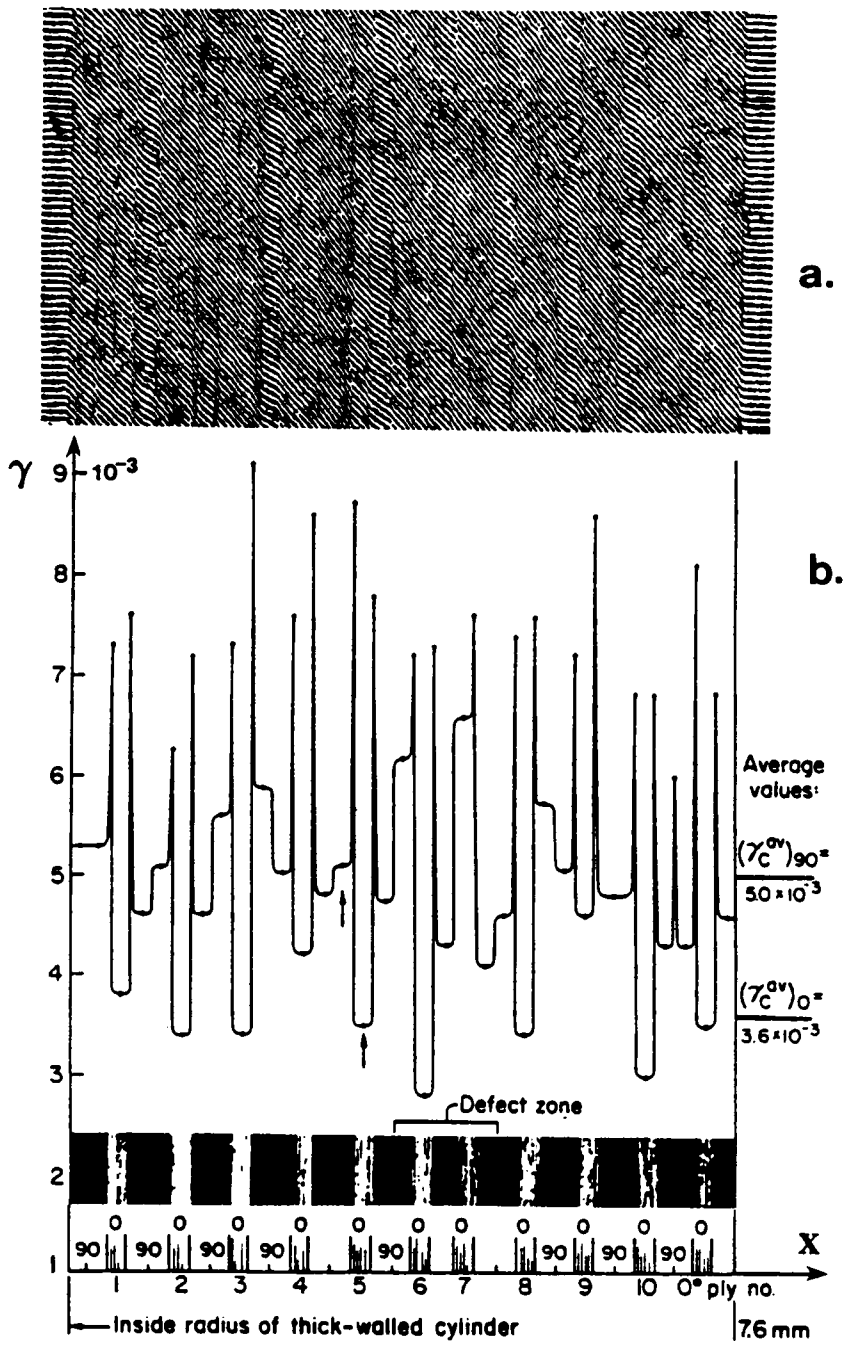

Fig.2-5. Carrier fringes are used to increase the resolution of fringe gradients in the test of Fig.2-4. a. Load-induced fringes with carrier fringes of extension. The slopes show the shear strain levels. b. Actual strain distribution, which reveals high shear strains in the resin-rich zones between plies.

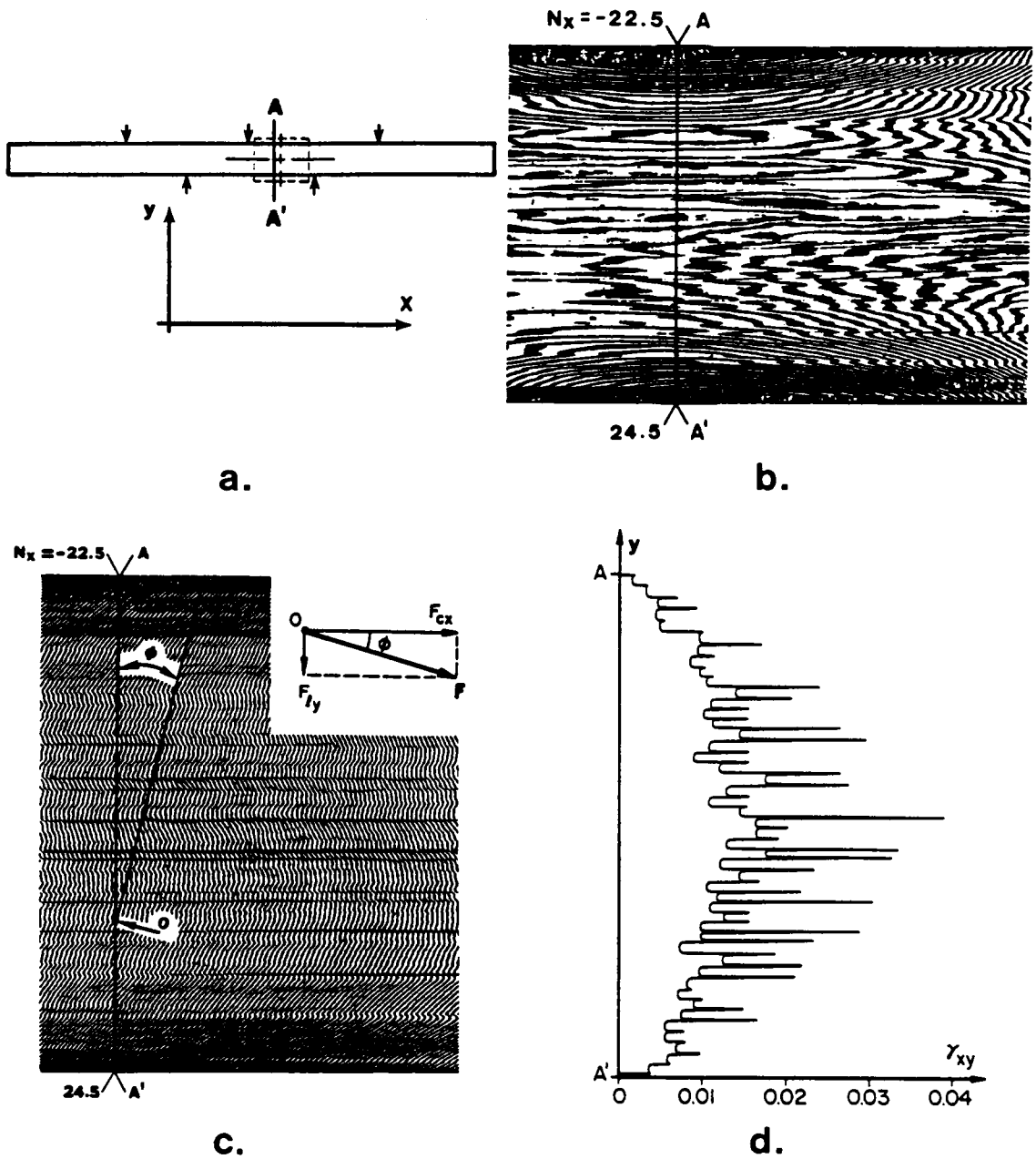

Fig.2-6. Five-point bending beam test of [+45/0/-45/90]6s graphite-PEEK composite specimen. a. Specimen and loading. b. Load-induced fringe pattern of the U field for the portion of the specimen in dashed box. c. Load-induced fringes with carrier pattern of extension. d. Shear strain distribution along the line A-A'.

the central region with certainty. In addition, there are insufficient fringes in the central region to determine the strain in each ply. However, carrier fringes of extension F_{cx} transform the pattern to that of Fig. 2-6c. Now, the fringes can be traced without ambiguity. The gradient F_{fy} in the different plies, along AA′, can be determined from the fringe slopes by Eq. 2.1, where F_{fx} and F_{cy} equal zero; it reduces to $F_{fy} = F_{cx} \tan \phi$ as shown in the vector diagram (Fig. 2-6c) for point O. The shear strain distribution along line AA′ was calculated by Eq. 1.5 and plotted in Fig. 2-6d, using data from this pattern and the corresponding V field. Again, the different strain levels in successive plies are caused by their different stiffness in shear. The high peaks occur at the resin-rich zones between plies, where high shear compliance leads to localized high shear strains.

2.6.2 The compression properties of composites

Figure 2-7 illustrates an interlaminar compression test of a thick composite. The material was graphite/epoxy with a [90/90/0]n stacking sequence, i.e., two plies with fibers in the z direction followed by one ply with fibers in the x direction, repeated many times. The specimen was 15 mm tall with 13x13 mm cross-section. The specimen was loaded in compression and the V field (vertical direction) displacement is studied to determine the normal strains in the y direction.

The load-induced fringe pattern of the V displacement field is shown in Fig. 2-7a for the portion in the dashed box. The strains could be determined easily in the 90 deg plies, by $\varepsilon_y = F_{fy} / f$. In the 0 deg plies, however, the fringes are too few to determine their gradient. In Fig. 2-7d, the dashed curve shows the normal strain distribution along the vertical centerline of the specimen as extracted directly from the load-induced fringe pattern in Fig. 2-7a. Large strain concentrations cannot be resolved from this pattern because of the lack of resolution of fringe gradients.

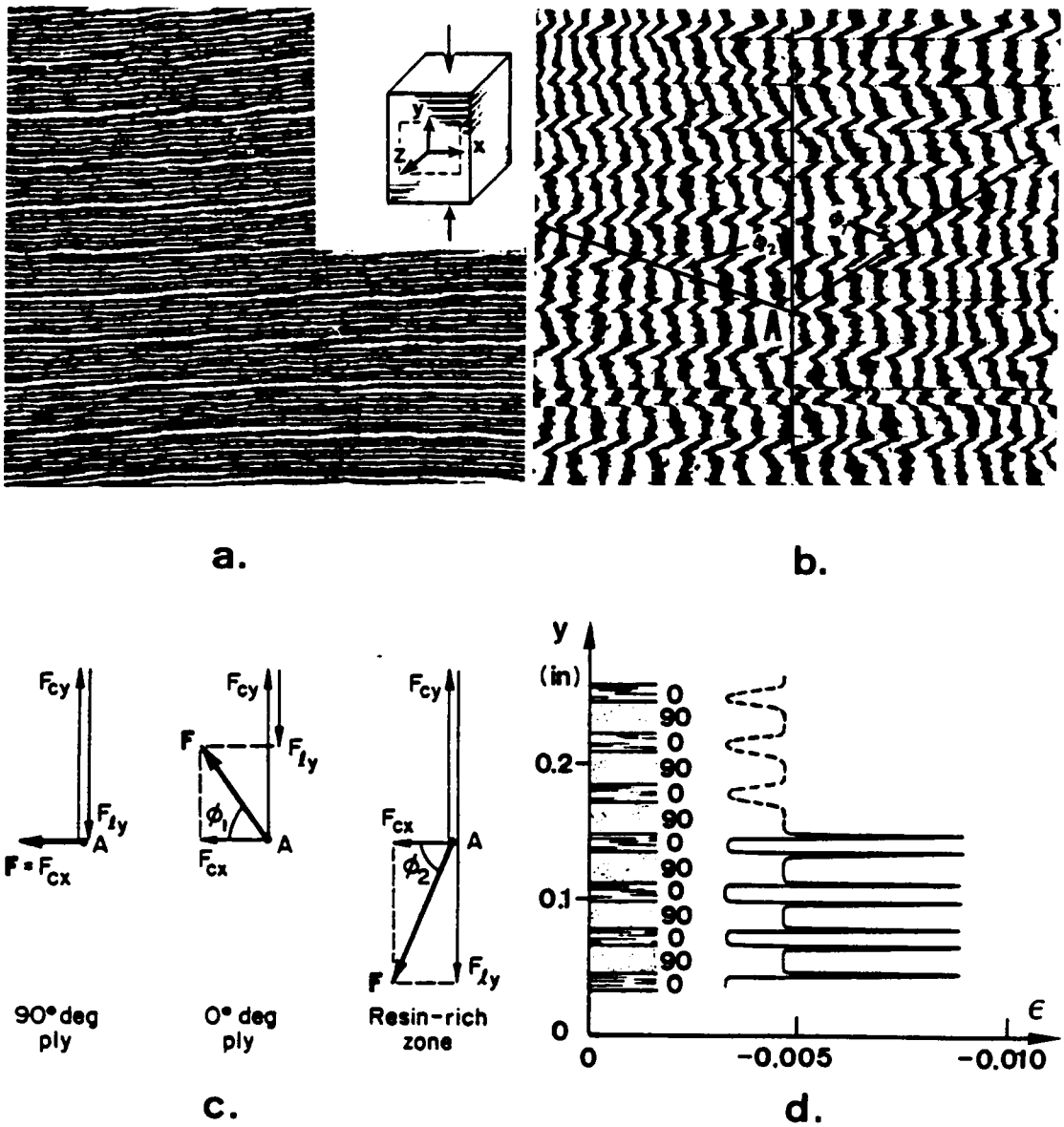

Fig.2-7. Interlaminar compression test of [90/90/0]n graphite/epoxy composite specimen. a. Load-induced fringe pattern of the V field for portion of the specimen in dashed box, b. Load-induced fringes with carrier fringes of extension and rotation. c. The vector diagram. d. Apparent strain distribution (the dashed curve), which dose not show the existing strain concentrations and the Actual strain distribution (the solid curve), which reveals the high compressive strains in the resin-rich zones between plies.

The pattern was transformed to that of Fig. 2-7b by adding carrier patterns of both extension and rotation. First, a carrier pattern of extension was applied; it was equal in magnitude and opposite in sign to the fringe gradient in 90 deg plies, such that the fringe gradient in 90 deg plies was cancelled (or in some regions, nearly cancelled). Then a carrier pattern of rotation was applied to produce Fig. 2-7b. Near point A, the fringes in 90 deg plies are vertical, which indicates that the y component of the resulting fringe vector is zero. In 0 deg plies, the fringes have an azimuth ϕ_1 and in resin-rich zones between plies they have an azimuth ϕ_2. The corresponding strains ε_y are calculated by using Eqs. 2.1, 2.3 and 1.4, from which

$$\varepsilon_y = \frac{1}{f} F_{cx} \tan\phi + \varepsilon_{90} \quad ; \qquad \varepsilon_{90} = -\frac{1}{f} F_{cy} \tag{2.8}$$

where ε_{90} is the normal strain in the 90 deg plies, i.e., the strain that was subtracted off by introducing $F_{cy} = -F_{ly}$. Equation 2.8 is an implementation of Eq. 2.1 when both $F_{cx}$and F_{cy} are non-zero.

The pattern of Fig. 2.7b is interpreted by fringe vectors in Fig. 2.7c. In 90 deg plies, F_{ly} is known; therefore F_{cy} is known. F_{cx} equals the resultant horizontal vector and its magnitude is determined by measuring the horizontal distance between fringes in Fig. 2.7b. The carrier fringe vector F_{cx} and F_{cy} are constants throughout the pattern, and their magnitudes are known. For the 0 deg ply near point A, F_{cy}, F_{cx} and the azimuth ϕ_1 of F are drawn. The vector diagram is readily completed, thus establishing the magnitude of F_{ly}, and by Eq. 1.4, establishing ε_y in the 0 deg ply. Note that the direction of F is verified, because it is known from Fig. 2.7a that F_{ly} must be smaller in magnitude in 0 deg plies than in 90 deg plies.

Narrow zones between plies exhibit fringes of azimuth ϕ_2. These represent resin-rich zones that are more compliant in compression than the neighboring plies. The

vector procedure is the same. With F_{cx}, F_{cy} and ϕ_2 known, the diagram is completed by drawing the unknown vector F_{ly}. The results are plotted in Fig. 2.7d, which shows essentially uniform compressive strains through the thickness of each ply and strong strain peaks in the resin-rich zones between plies. Clearly, this detail cannot be obtained from the load-induced pattern without the use of carrier fringes.

2.7 Conclusions for Chapter 2

Usually, if more data points are needed between two neighboring fringes, a complicated technique, such as grey level recognition, has to be employed. The carrier fringe technique provided equivalent results with a very simple procedure.

Information that can be extracted from moire patterns is vastly increased by using the carrier fringe technique to improve the resolution of fringe gradients. High strain concentrations which cannot be recognized in a load-induced fringe pattern are easily observed in the carrier fringe-added fringe pattern. The procedure of extracting the data is also much easier and more accurate.

The carrier fringe technique in moire interferometry is very powerful in micromechanics measurements for composite materials. The deformations in the plies and between the plies can be obtained with high accuracy. The deformations in an individual fiber and in the matrix between the two neighboring fibers can also be determined when the microstructure is relatively coarse.

Fringe vectors provide an effective means of interpreting the patterns. The carrier patterns are easily introduced and controlled by adjustments of the moire interferometry optical system.

3.0 New Moire Interferometers

In this chapter, according to the objectives, new moire interferometers will be introduced. These systems are relatively insensitive to the vibrations and can be operated off the optical table, for example, in the material testing laboratory. This development is very important in expanding the applications of moire technique to the broad experimental study of the properties of various materials and structures.

3.1 Introduction

Moire interferometry has very high sensitivity to the displacement in the direction of the measurement, the direction perpendicular to the lines of the reference grating [33]. Usually, it has the same sensitivity to the noise, for example the vibration, in the same direction. The system shown in Fig. 3-1 is designed for measuring the displacement in the x direction, so that it is very sensitive to the vibration in the x direction between the specimen grating and the virtual reference grating.

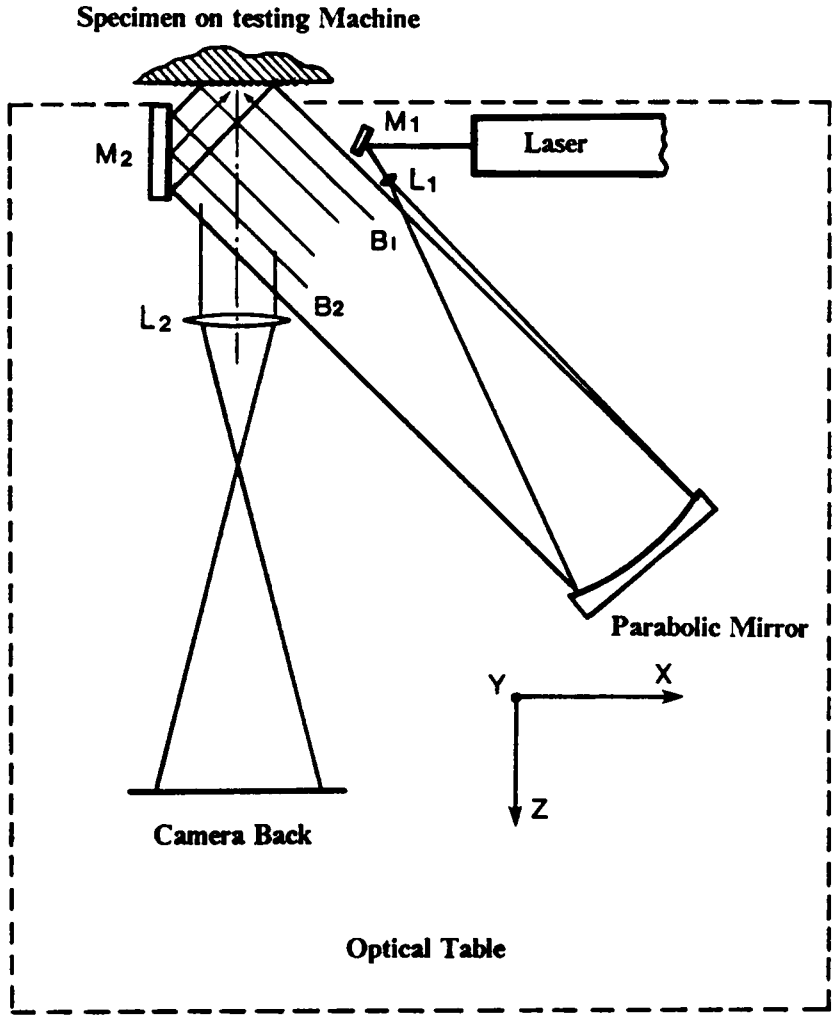

Fig. 3-1. Optical setup of a linear moire system where the specimen is separated from the optical table.

Usually, the experiments are operated in the optical laboratory with all the optical elements and the specimen attached to the optical table in order to minimize vibrations and to obtain stable fringe patterns. When special conditions are required, such as high loads and large test structures, the experiments have to be performed off the optical table. For example, if the optical system which generates the virtual reference grating is placed on an optical table and the specimen (with specimen grating) is loaded by a testing machine, the vibration between the optical table and the testing machine, which introduces the relative motion between the illuminating system and the specimen grating, will influence the contrast of fringes severely. So far, two major methods have been used to deal with the vibration problems in order to get clear fringe patterns. One is to freeze the motions by very short exposure time when the fringe patterns is photographed, and the second one is to synchronize the motions by attaching the sensitive optical elements of the interferometer on the specimens. The first method, which has been successfully used in the dynamic moire [34], does not have the quality of real time observation and is extremely expensive. In performing the static tests, the second approach is much more practical. The ideas and systems presented in this paper are all those using the second approach, which is synchronizing the motion by attaching the optical elements, such as mirrors and gratings, to the specimens.

In a regular moire system (Fig. 3-1), the mirror (M_2), which is used to direct the beams to form the virtual reference grating, is placed in the optical system together with the light source (Laser) and the other optics such as beam expander (L_1) and collimater (Parabolic Mirror). When the specimen is loaded on a loading frame separated from the optical system, the vibrations between the two bodies, the illuminating system and the loading frame, will severely affect the visibility of the fringe pattern. If the mirrors are removed from the illuminating system and attached to the specimen on the loading frame, the situation will be totally different. Such systems will be introduced.

The real reference grating method has been used for different purposes in moire interferometers. The major applications were in the fringe multiplication method and achromatic interferometers [22,35,36]. Although the real reference grating was used to redirect the incident light in the one beam moire system [10,37], the applications in eliminating vibration effects were not discussed. In the following chapter, a theoretical analysis is provided to explain how real gratings can be used to create a vibration insensitive moire system. Various options are discussed and the experimental variations are provided.

3.2 Kinematic Properties and Their Influence

In moire interferometry, the objective is to measure specimen deformations. The rigid body motions, like vibrations, have the same dimensions as the measured quantities and they add noise to the output of the system. In three-dimensional space, rigid body motion has six degrees of freedom. They are three translations and three rotations as shown in Fig. 3-2. The optical system used to form the virtual reference grating and the specimen with the specimen grating can be considered as the two bodies in the rigid body motion problem. The relative movements between them has six possibilities according to the six degrees of freedom of rigid body motion. The output of a moire system, the fringe pattern, is determined by the input which is the relative motion between the specimen grating and the reference grating.

Not all the six motions are critical to the output of a moire system. The key is to recognize them and deal with them properly.

In Fig. 3-2, the six motions of the specimen grating relative to the reference grating are:

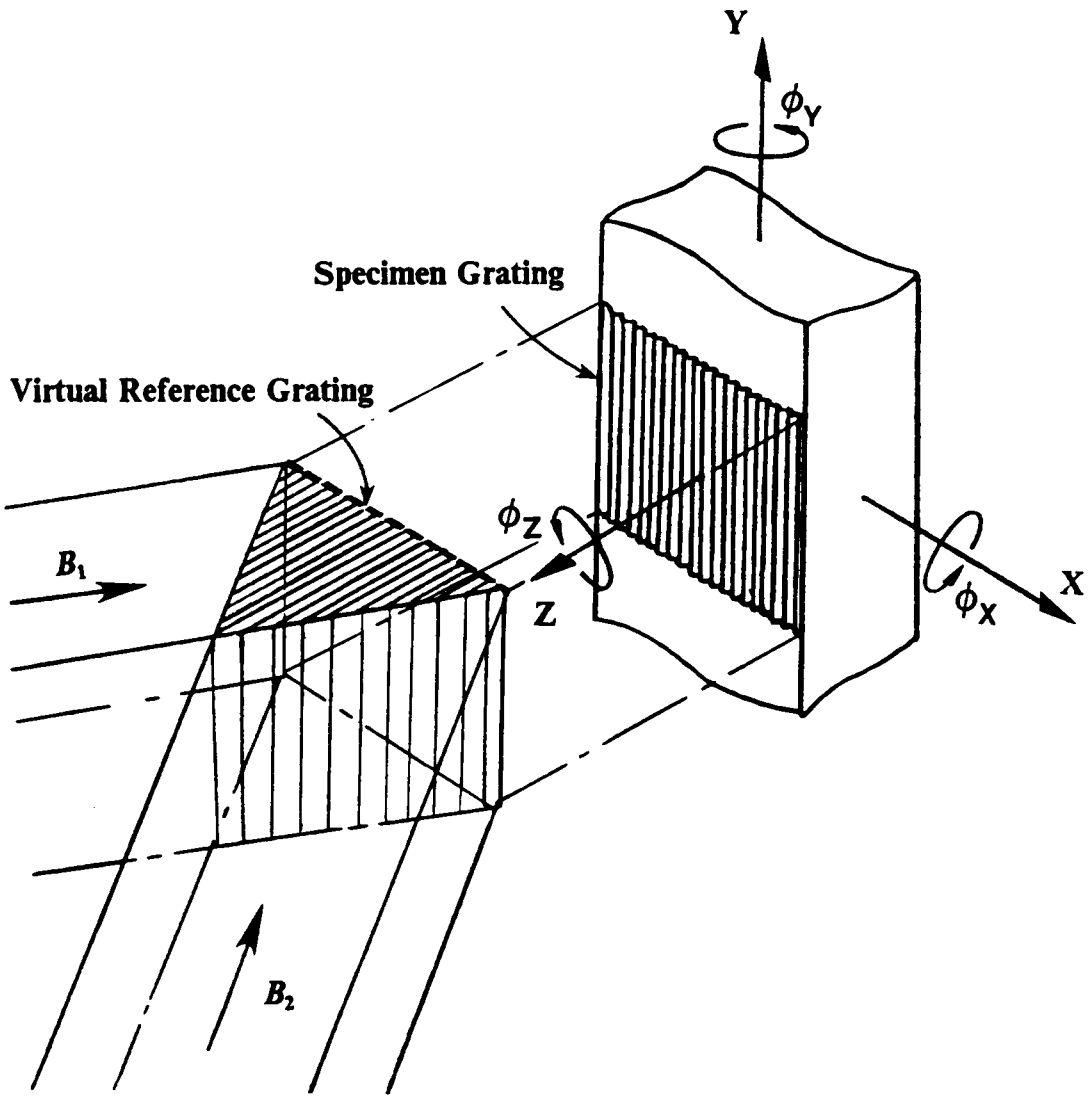

Fig. 3-2. Rigid body motions between the specimen grating and the virtual reference grating are the three translations (x, y and z) and the three rotations (ϕ_x, ϕ_y and ϕ_z).

a. Translation in x direction: The system has very high sensitivity to the motion in this direction because it is built to measure the displacement in this direction. If the frequency of the reference grating is 2400 line/mm, a specimen displacement of 0.2 micrometer in this direction will create a phase difference of 180 deg between the two output beams I_1 and I_2 (Fig. 1-3) and change the constructive interference to destructive interference (or vice versa) in the fringe pattern. If the displacement is cyclic, such as a vibration, the contrast of the fringe pattern will be washed out completely and the average intensity distribution will be uniform.

b. Translation in y direction: A linear system which has its grating lines parallel to the y axis is completely insensitive to displacements in the y direction. When the specimen grating moves relative to the reference grating in this direction, there is no phase change introduced to the diffraction beams I_1 and I_2 , so that the interference pattern (fringe pattern) remains unchanged.

c. Translation in z direction: This is the out-of-plane motion. A moire system of in-plane displacement measurement, as shown in Fig. 3-2, is completely insensitive to the out-of-plane displacement. When the specimen moves back and forth, the phase change introduced to the diffraction beams I_1 and I_2 is the same for both beams. Therefore, the phase difference between those two beams remains constant and the fringe pattern is stable.

d. Rotation around x axis: The displacement introduced by a small out-of plane rotation ϕ_x at an arbitrary point on the specimen surface can be decomposed into two linear components ΔV and ΔW as shown in Fig. 3-3a. The system is insensitive to both of the components as mentioned in (b) and (c). Therefore, the system is insensitive to the rotation in this direction.

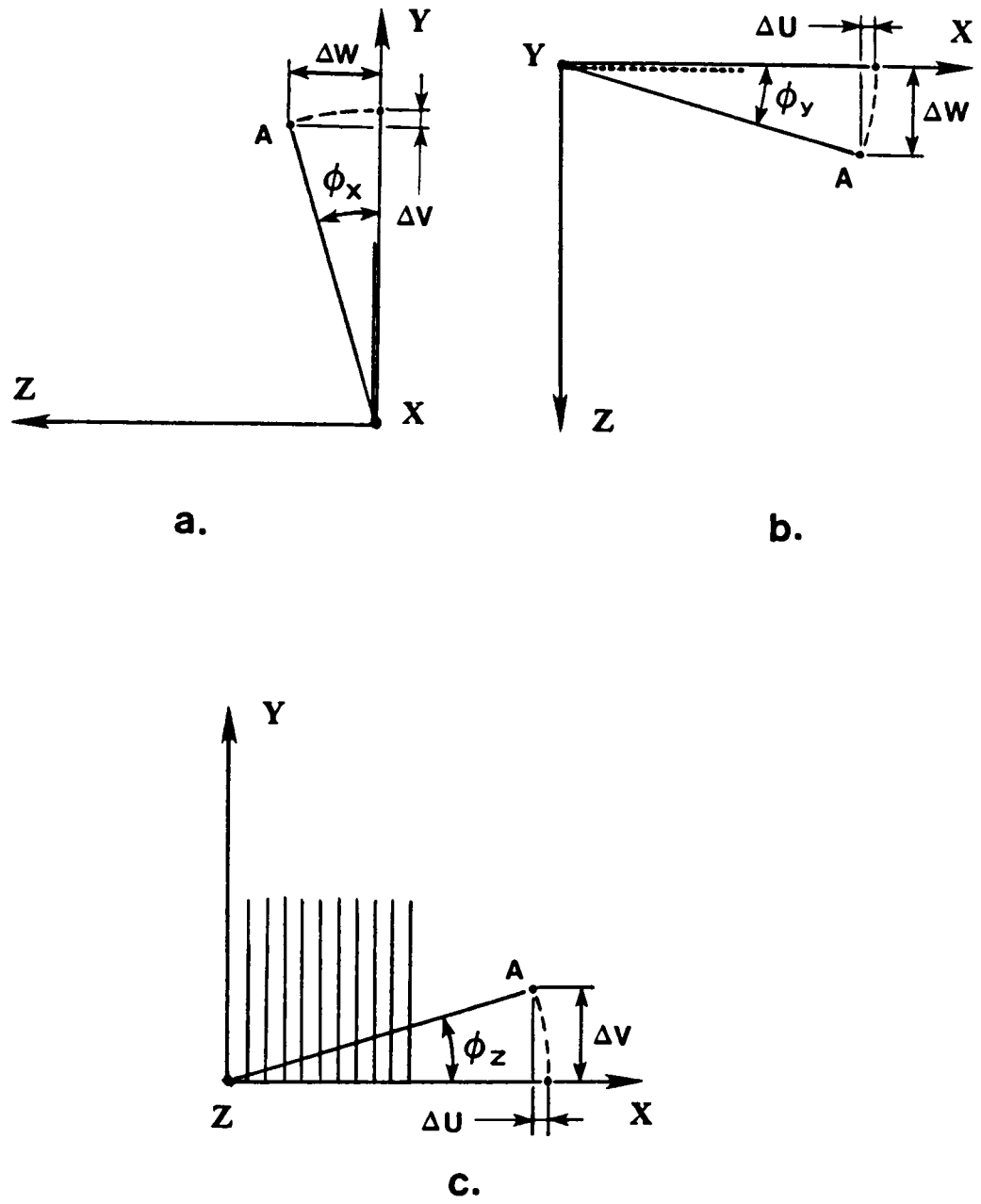

Fig. 3-3. Sensitivities of a moire system to the rotations of the specimen grating. a. Rotation around x axis. b. Rotation around y axis. c. Rotaion around z axis.

e. Rotation around y axis: The influence of the out-of plane rotation in this direction can also be decomposed into two linear displacements ΔU and ΔW. As shown in Fig. 3-3b, for a small rotation of angle ϕ_y, the arbitrary point A will move to point A1 and experience a displacement of ΔU and ΔW. Since the system is very sensitive to the x direction displacement, this rotation can be detected because of the associated displacement ΔU. The displacement component in the z direction cannot be sensed by the system as mentioned in (c).

The linear displacement ΔU introduced by out-of plane rotation ϕ_y is usually negligible because the magnitude is very small. For example, in a regular moire system, when $\phi_y = 0.01$ m/m, the extraneous fringe gradient is 0.12 fringes/mm [20]. This means that if there is a rotation vibration, its influence on the stability of fringe pattern is very limited.

f. Rotation around z axis: The system is sensitive to this rotation, ϕ_z. It can be detected by the system because there is an associated displacement ΔU. As shown in Fig. 3-3c, this is the in-plane rotation and can be decomposed into two components ΔU and ΔV. The system has high sensitivity to this rotation because there is an associated U displacement component, and this linear displacement has the same magnitude as the rotation itself. Actually, one of the shear strain components is measured by this sensitivity to the in-plane rotation.

The conclusion is that any relative motion between the specimen and the virtual reference grating which involves displacements in the x direction, ΔU, will be sensed by the linear moire system in Fig. 3-2. If there exists a vibration and its magnitude has a component in the x direction, the output of the system will be affected. Consequently,

if the magnitude of this component is equal to or greater than 0.417/2, the contrast of the fringes will be lost completely.

To perform off table moire, for example on the testing machine, the specimen is usually separated from the illuminating system which is used to form the virtual reference grating. The vibration between the specimen grating and the virtual reference grating will be the noise, which can wash out the contrast of the fringe pattern. One way to solve this problem is to set the optical system on the testing machine together with the specimen. However, the optical system frequently cannot be held on the testing machine nor can it be attached stiffly enough to eliminate the vibration.

Instead of eliminating the relative motion between the specimen grating and the reference grating to obtain the stable fringe patterns, the same goal can be achieved by reducing the sensitivity to this relative motion. In the following section, a new idea is introduced to design the off-table moire systems that reduce the system's sensitivity to the relative vibration.

3.3 Sensitivity to Vibrations

Generally, in a system of measurement, the sensitivity to the noise is equal to the sensitivity of the measurement. A linear moire system is only sensitive to the motion in one direction and the sensitivity is 0.417 micrometer per fringe order if it has a reference grating of 2400 lines/mm. This sensitivity is a function of the frequency of the reference grating and this frequency depends on the intersection angle between two coherent beams which create the virtual reference grating. Therefore, the sensitivity can be expressed as a function of the angle of intersection α (by using Eq. 1.2):

$$S = \frac{\lambda}{2 \sin \alpha} \qquad (3-1)$$

where λ is the wavelength of the incident beams B_1 and B_2 and α is half of the intersection angle between those two beams (Fig. 1-3). In a regular moire system, Fig. 3-4a, if the helium-neon laser is used (λ = 633 nm), the half angle α is about 49.4 deg, and the sensitivity to the vibration is 0.417 micrometer displacement per fringe order. The magnitude of the displacement (per fringe order) is equal to G, one pitch of the reference grating. A relative motion between the specimen grating and the reference grating by this amplitude will cause one fringe order shift in the fringe pattern. When the intersection angle between two incident beams is reduced, as shown in Fig. 3-4b, the displacement needed to make one fringe order shift is increased because the pitch of the reference grating G is increased. Therefore, the sensitivity is reduced. If the incidence angle is 10 deg, the sensitivity is 1.822 micrometer per fringe order. The sensitivity is proportional to $\sin \alpha$. When the incidence angle is close to zero, the sensitivity reduces very rapidly. In the systems shown in Fig. 3-4, when sensitivity to the vibration is reduced, the sensitivity of the measurement is reduced too. The goal here is to reduce the sensitivity to the vibration but keep the high sensitivity to the measurement.

3.4 The Idea

As introduced before, the sensitivity of a moire system is determined by the intersection angle of the two incidence beams. In Fig. 3-5, the incidence angle (2α) is very small, so that the sensitivity to vibrations between the incidence beams and the specimen grating is low. To achieve the high sensitivity for measurement, an optical element is

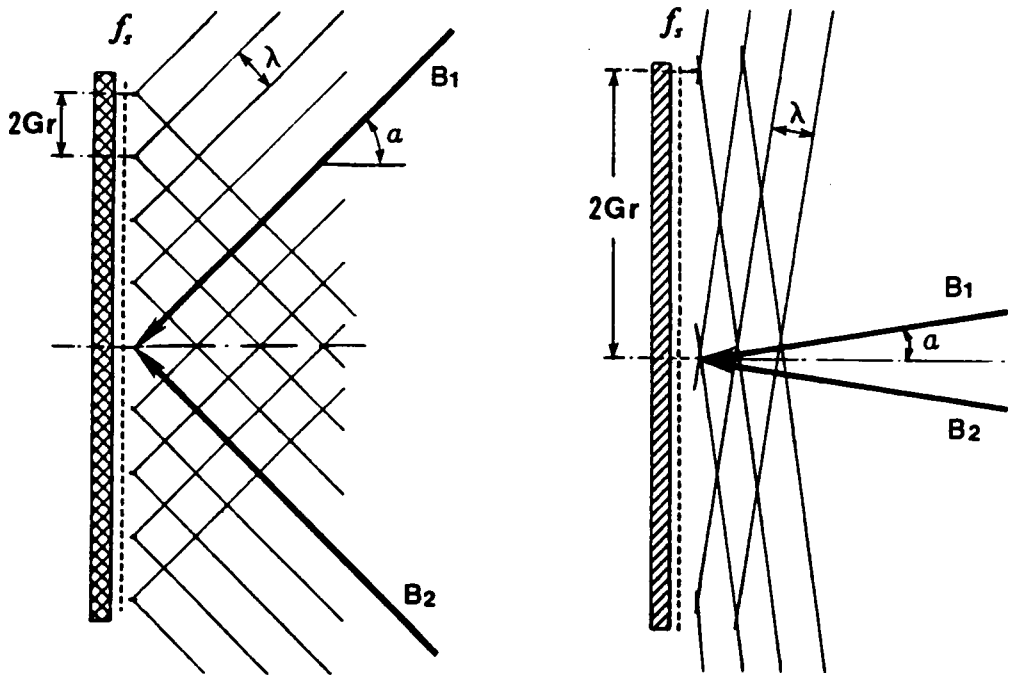

Fig.3-4. The sensitivity of a moire system is a function of the incidence angles of two coherent beams which create the reference grating. a. A regular moire system, where the incidence angles are 49.4 deg and sensitivity is 0.417 micrometer per fringe order. b. A moire system with reduced sensitivity, where the incidence angles are smaller.

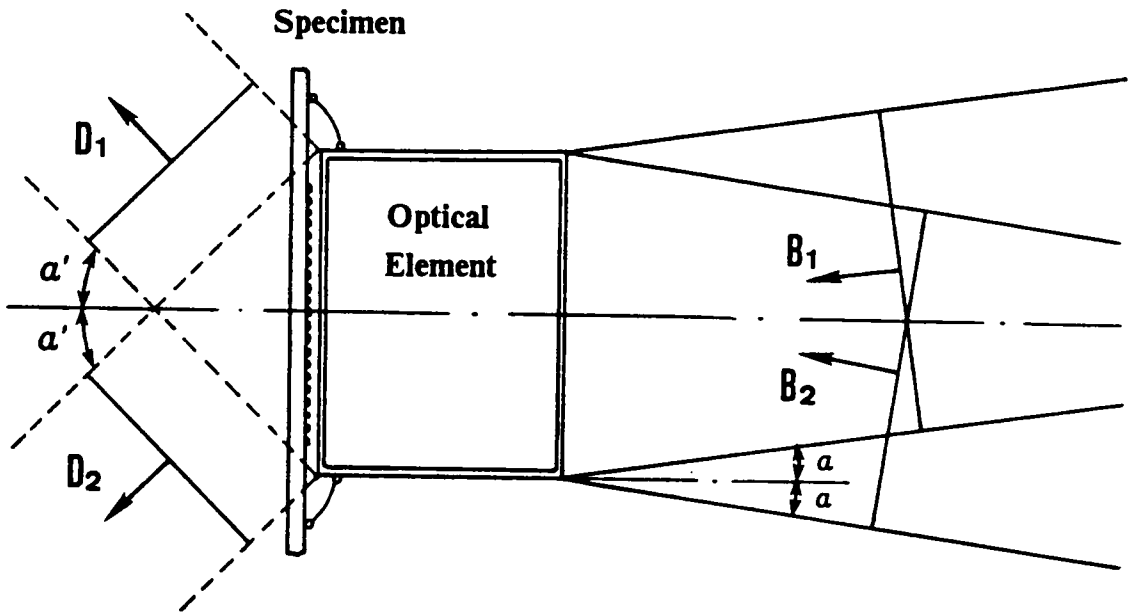

Fig.3-5. An attached optical element can be used to redirect the incident beams and reform the high sensitivity for measurement.

used to redirect the incidence beams B_1 and B_2 right before they strike the specimen grating. A large incidence angle α' is reformed and a high frequency virtual reference grating is created in front of the specimen grating. The attached optical element is mounted in such a way that it does not vibrate relative to the specimen, so that there is no noise generated even though the sensitivity there is very high. This optical element could be a mirror, a prism or a real grating.

Once the sensitivity to the vibration is reduced, the contrast of the fringe pattern will improve when experiments are performed in a vibration environment. The system will be able to tolerate relative vibrations between the specimen and the optical system sufficiently well to be used off the optical table.

3.5 A Three Mirror System

The system, depicted in Fig. 3-6, has three mirrors attached to the specimen such that there is no relative motion between the specimen and the mirror system. The U and V displacement fields can be measured simultaneously. When the U displacement field is measured, the two incident beams B_1 and B_2 have zero angle of intersection before they reach the specimen and the attached mirror M_1. The sensitivity to vibrations is theoretically zero between the illuminating system (the incident beams) and the system that consists of the specimen and the mirror. The large intersection angle is obtained in front of the specimen when one of the incident beam hits the mirror and changes its direction. Accordingly, the high sensitivity to the measurement is reformed. When the V displacement field is measured, the incident beams are redirected symmetrically by two mirrors (M_2 and M_3) before they reach the specimen grating. The high sensitivity is achieved after the incident beams are redirected. The relative movements between the

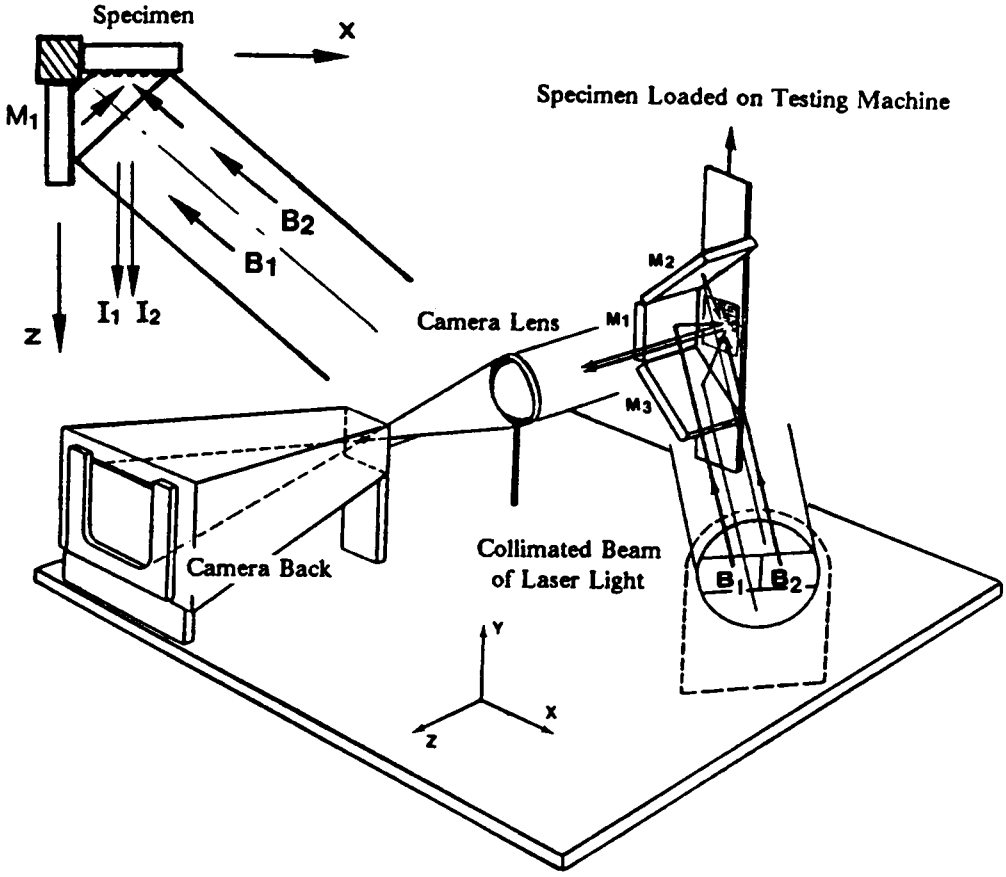

Fig. 3-6. A three mirror moire system. Mirrors are attached to the specimen to reduce the influence of vibrations.

specimen grating and the virtual reference grating are eliminated because the mirrors are traveling together with the specimen. The principle can also be explained by the phase change in the information beams. For example, if the U field is measured, the motion of the specimen in x direction, together with the mirror, will change the optical path lengths of two incident beams B_1 and B_2 by the same amount, so that there is no phase difference introduced by the motion. Consequently, there is no phase change between the two diffraction beams I_1 and I_2 which form the fringe pattern, and the fringes are stable. Because the system, when the U field is measured, is also insensitive to the y and z direction vibrations, it is, therefore, insensitive to all linear vibrations. The situation is the same when the V displacement field is measured. With this property, the capability of adapting to the environment is greatly increased.

The rotational movements of the specimen, together with the mirrors, introduce carrier fringes to the fringe patterns. The system cannot be used to measure the absolute values of strains. Since carrier fringes produce constant apparent strains, they have no influence on relative values of strains, and the method is good for determining the strain variations. Another shortcoming of this system is that in order to obtain both U and V displacement fields, three mirrors have to be attached to the specimen. For small specimens, the weight of the mirrors may have an influence on the loading conditions, even if each mirror is tailored to the exact shape and size needed to illuminate the test area.

3.6 Real Reference Grating Methods

A real reference grating can be attached to the specimen and used to redirect the incident beams.

3.6.1 Scheme 1, a one-beam moire interferometer

This new system with low sensitivity to vibrations is developed from the idea of a one-beam system shown in Fig. 3-7. Actually, this incident beam B will be divided into two beams to form the virtual reference grating. Since, before they are divided, the two beams travel in the same direction, they can be considered as a single beam. A real reference grating f_r, a transmission grating, is attached to the specimen grating f_s with a small clearance. It travels with the specimen grating and experiences the same rigid body motions but does not deform with the specimen. The relative vibration between the two gratings is eliminated by the synchronized motions. The system can be divided into two parts. One consists of the specimen grating and the real grating, and the other one consists of the optical system which forms the collimated incident beam B. The specimen grating is illuminated by the beams D_1 and D_2. Before they reach the real grating, beam D_1 and D_2 , as a single beam, has zero angle of intersection, so the sensitivity to vibrations between the real grating and the incident beam B is theoretically zero, as analyzed before. The system is considered as two rigid parts, and the vibration can only happen in between them. Because the sensitivity is zero between those two rigid parts, the system is insensitive to the vibration. After passing through the real grating, beam B is divided into two beams and redirected by the incident angle α'. The high sensitivity to the measurement is reformed.

Unfortunately, this system is not practical because of the difficulties of separating information beams I_1 and I_2 from the beams that reflect directly from the real grating surface and the specimen surface. These reflected beams have much higher intensity than diffracted beams I_1 and I_2, and they will enter the camera together. The information cannot be separated from the strong background light. In addition, this system does not

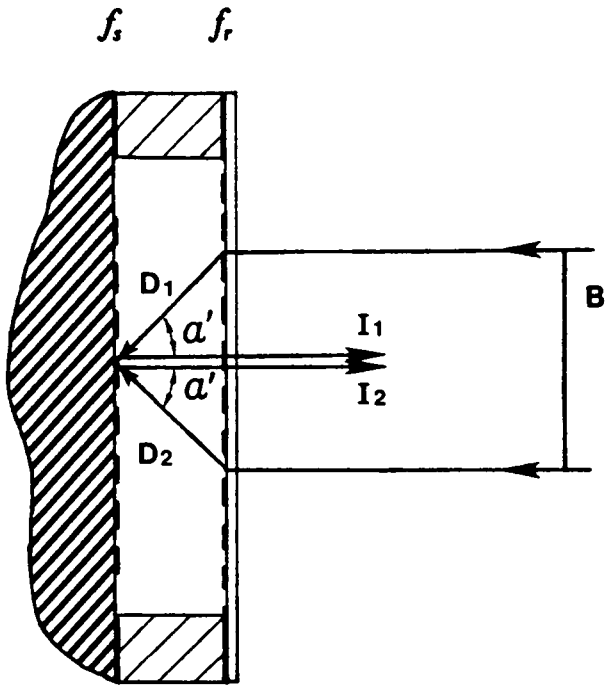

$$f_r = f_s = 1200 \ lines/mm$$

Fig. 3-7. Schematic ray diagram of one-beam system with normal incidence.

have the capability of adjusting the initial null-field and introducing carrier fringes because the frequency of the virtual reference grating cannot be changed.

3.6.2 Scheme 2, a two-beam system with symmetrical incidence

Although it is not a practical system, the interferometer in scheme 1 provided the valuable inspiration for designing a system with reduced sensitivity to vibrations. The practical system is developed by introducing a small angle between the two incident beams B_1 and B_2 , as shown in Fig. 3-8. Two collimated beams (beam B_1 and B_2) are used to illuminate the real grating f, symmetrically. In practice, the two incident beams can be directed by two separate mirrors which are fixed on a rigid fixture together with the other optics and the light source. The relative motion between the two beams B_1 and B_2 is limited by the small separation of the two mirrors and the rigid fixture. Vibrations may appear between the real grating f, and the incident beams B_1 and B_2. However, the sensitivity there is low because the intersection angle 2 α between those two incident beams is very small. Again, the high sensitivity to the measurement is reformed by the real grating as the incident beams are redirected with a large incidence angle α'.

By adjusting the incidence angle α, the system is able to obtain null-field and to introduce carrier fringes, just as a regular moire system. The information beams are well separated from the direct reflection beams because the reflection beams now have a deviation from the normal direction. The information beams are received by the camera through the gap between the two mirrors M_1 and M_2 (Fig. 3-8). This system is called a two-beam symmetric system in order to distinguish it from the others.

In a two-beam system as shown in Fig. 3-8, when a small angle α is used, the system has to be modified in order to get the incident angle α' to match the frequency of the specimen grating, so that the first order of the diffraction beam will emerge normal to

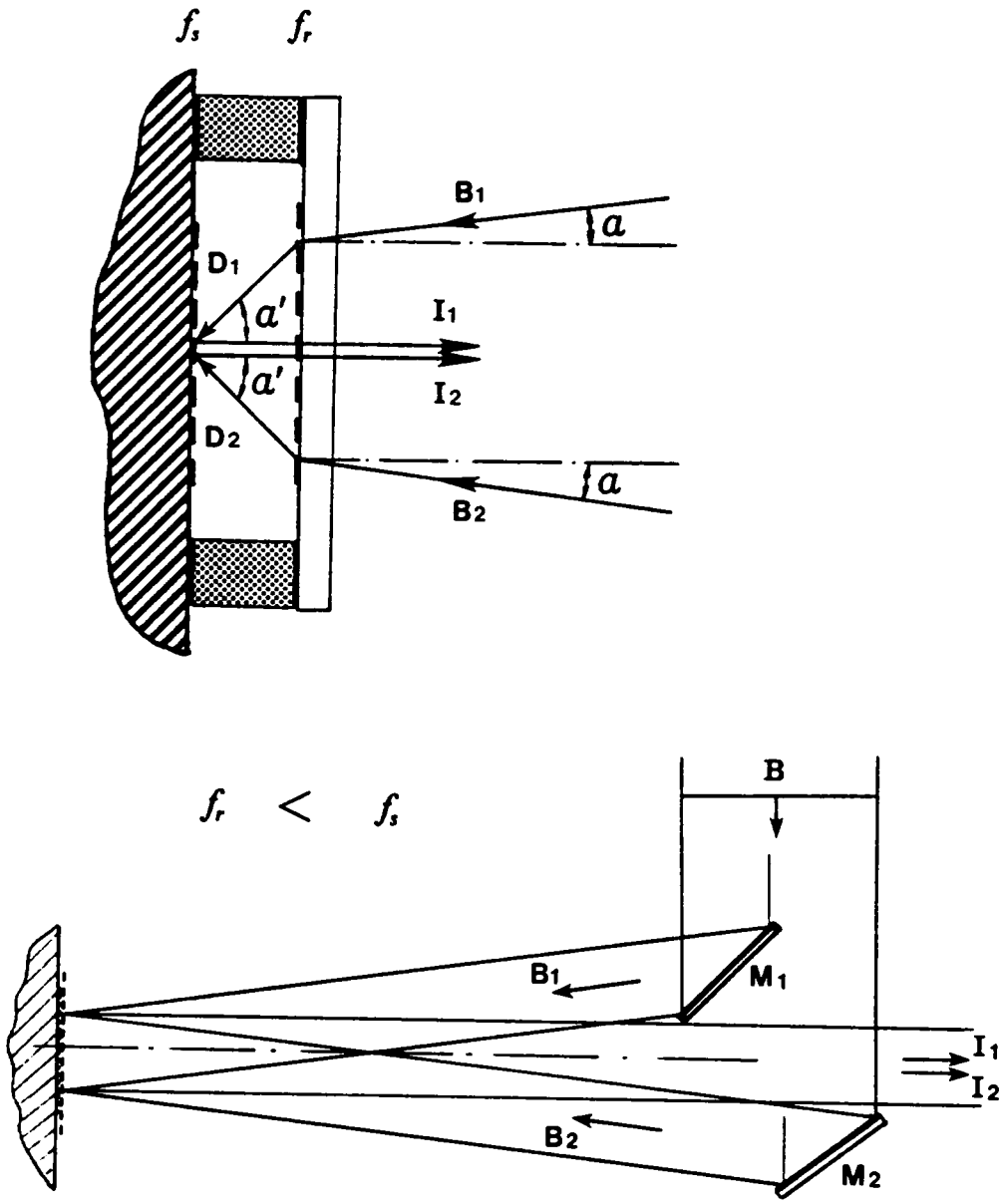

Fig. 3-8. Diagrams of a two-beam system with symmetric incidence.

the specimen surface. Two techniques can be applied. One introduces a frequency mismatch between the specimen grating and the reference grating, and the other one introduces a rotation mismatch between the two gratings.

The first technique, a frequency mismatch, is illustrated in Fig. 3-9. The amount of mismatch introduced can be determined by the incident angle α. Here, α is 5 deg and the frequency of the reference grating is 1062 lines/mm, 138 lines less than the specimen grating. The sensitivity to the vibration is reduced to 11% of the regular interferometer which has an incident angle of 49.4 deg.. This is an order of magnitude improvement. The further reduction of the incidence angle is limited by the consequent reductions of the range of measurement, the size of test area and the adjustability. For example, if a strain of magnitude of 0.2 is measured, the corresponding frequency of fringes is 130 lines/mm and the diffraction angle between the two information beams is 4 deg. In order to separate those two beams from the incident beams, the intersection angle of the two incident beams has to be larger than the divergence angle of the two information beams. In addition, the image of the fringe pattern has to be received in between the two incident beams. This requires that the distance between the two mirrors (M_1 and M_2 in Fig. 3-8) is larger than the size of the specimen grating.

The second technique using a rotational mismatch is shown in Fig. 3-10. By rotating one grating relative to the other by a small angle ψ, the same condition as using frequency mismatch can be achieved. The angle of rotation is a function of incident angle α. In the system (Fig. 3-10), α is 5 deg and ψ is 4.3 deg. For rotational mismatch, a reference grating which has the same frequency as the specimen grating can be used.

In Fig. 3-10, the specimen grating is shown to be rotated by a small angle ψ for convenience of explaining the optical principle. In practice, it is the real reference grating that is rotated by ψ relative to the specimen grating.

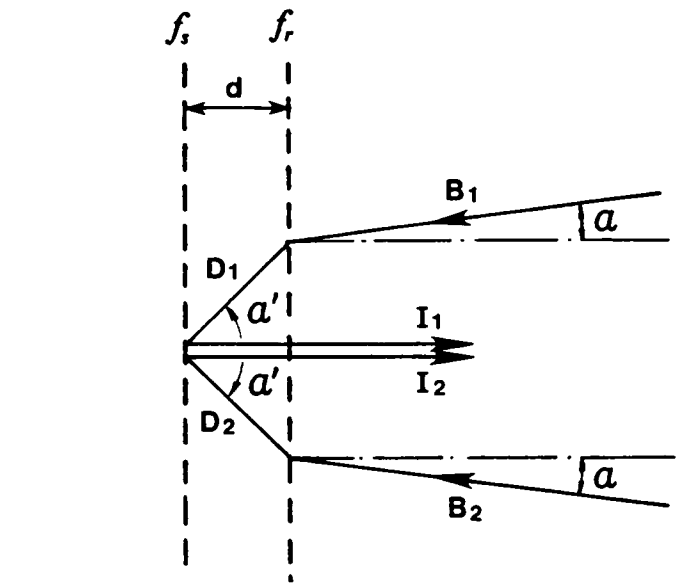

$f_r = 1062$ *lines/mm* $\quad f_s = 1200$ *lines/mm*

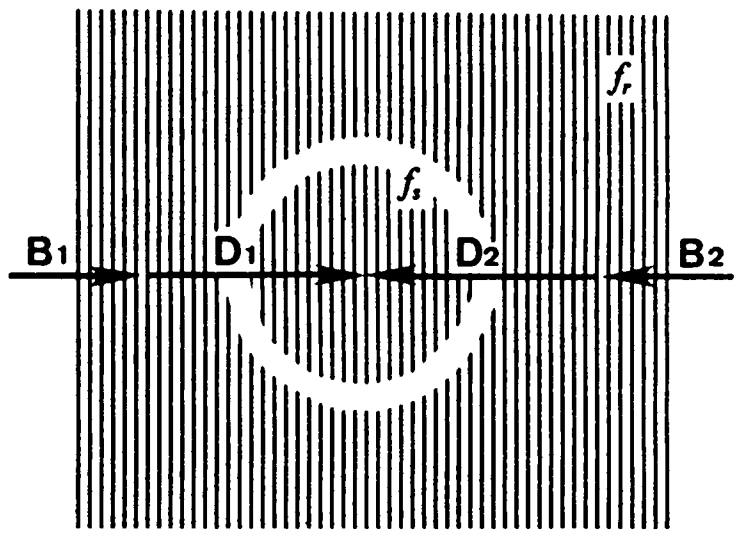

Fig. 3-9. Schematic ray diagrams for the new two beam system with frequency mismatch. By using symmetric beams with incidence angles of 5 deg, the sensitivity to the vibration is reduced to 11% of the regular moire interferometer.

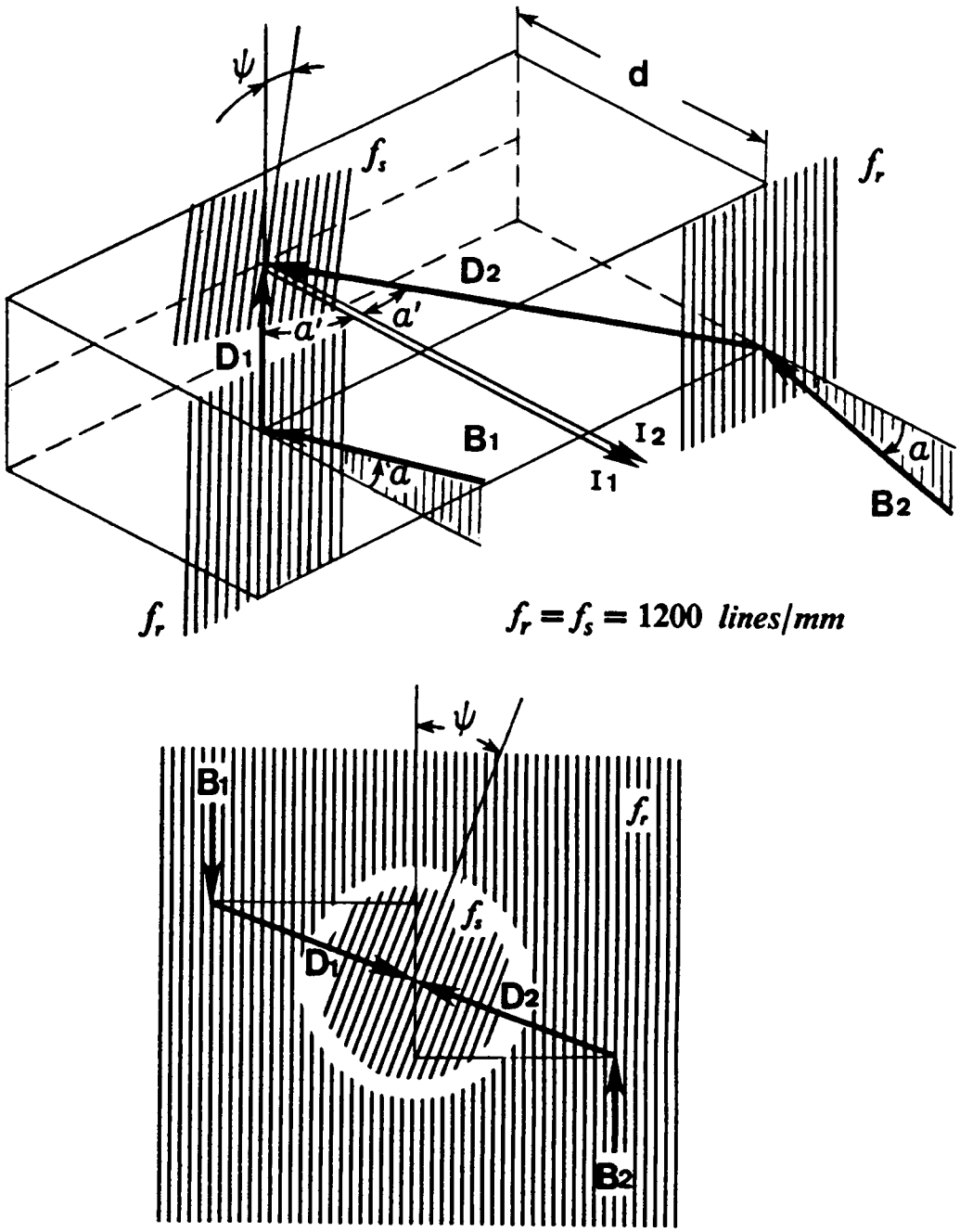

Fig. 3-10. Schematic ray diagrams of the new two-beam system with rotational mismatch. The sensitivity of vibrations is reduced when the small incidence angle α is used.

The extraneous diffraction orders

Although the problem of direct reflection is solved by introducing a small incidence angle α by either frequency mismatch or rotational mismatch, there is still more than one diffraction order from each incident beam that could enter the camera. As shown in Fig. 3-11, each incident beam is diffracted by the two gratings three times before it reaches the camera. For beam B_1 , the diffraction order sequences (1,1,0) and (0,1,1) enter the camera together with the same angle if the two grating surfaces are parallel. There is a difference of the optical path lengths between those two beams. It introduces a phase difference and creates fringe patterns at the image plane. The same condition exists for incidence beam B_2, and a multi-beam interference pattern is formed on the camera back. The intensity distribution of the four-beam interference can be expressed by their complex amplitudes.

The complex amplitudes of the four beams are:

$$B_{11} = A_{11}e^{i\mu} \quad ; \qquad B_{12} = A_{12}e^{i(\mu+\delta_1)} \tag{3.2}$$

$$B_{21} = A_{21}e^{i\nu} \quad ; \qquad B_{22} = A_{22}e^{i(\nu+\delta_2)}$$

where B_{11} is the (1,1,0) diffraction order from incident beam B_1 and μ is its phase angle. B_{12} is the (0,1,1) diffraction order from the same incident beam and δ_1 is the phase angle difference between the two diffraction orders B_{11} and B_{12} . As shown in Fig. 3-11, the phase angle difference is created by the difference of optical path length when those two beams travel through the two gratings. B_{21} and B_{22} are the two diffraction orders from the other incident beam B_2. ν and δ_2 present their phase angles which have the same meaning as μ and δ_1 for the beams B_{11} and B_{12} . A_{xx} is the amplitude.

For the sake of simplicity, assuming the four beams emerge with the same intensity, that is

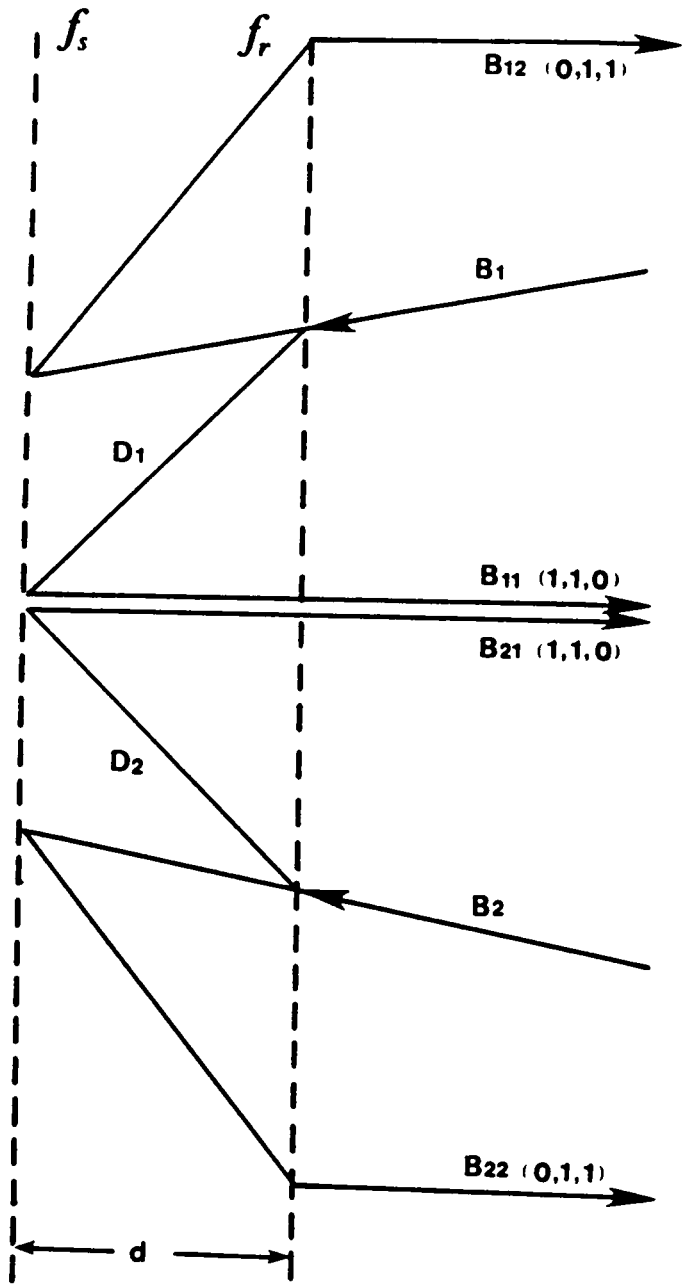

Fig. 3-11. The four diffraction beams from incidence beams, B_1 and B_2 will enter the camera. Two of them, B_{11} and B_{21}, interfere to form moire fringe pattern. Extraneous fringe patterns (noise) are added to the moire pattern because of the present of the diffraction orders B_{12} and B_{22}.

$$A_{11} = A_{12} = A_{21} = A_{22} = a \quad ; \tag{3.3a}$$

and assuming incidence beams B_1 and B_2 are symmetric with respect to the normal of the specimen surface and the two gratings are parallel, so that the phase angle difference of the diffracted beam from beam 1 should be equal to that from beam 2, that is

$$\delta_1 = \delta_2 = \delta \tag{3.3b}$$

Then Eq. 3.2 can be written as

$$B_{11} = a\, e^{i\mu} \; ; \qquad B_{12} = a\, e^{i(\mu+\delta)} \; ; \tag{3.4}$$

$$B_{21} = a\, e^{i\nu} \; ; \qquad B_{22} = a\, e^{i(\nu+\delta)} \; ;$$

and the intensity of the resultant interference pattern can be expressed as the product of the complex amplitudes and their conjugates

$$B = (B_{11} + B_{12} + B_{21} + B_{22})(B_{11} + B_{12} + B_{21} + B_{22})^{\star} \tag{3.5}$$

where the star indicates the complex conjugate.

The resultant intensity will have the following terms

$$B = a^2 \begin{bmatrix} 1 & e^{-i\delta} & e^{i(\mu-\nu)} & e^{i(\mu-\nu-\delta)} \\ e^{i\delta} & 1 & e^{i(\mu-\nu+\delta)} & e^{i(\mu-\nu)} \\ e^{-i(\mu-\nu)} & e^{-i(\mu-\nu+\delta)} & 1 & e^{-i\delta} \\ e^{-i(\mu-\nu-\delta)} & e^{-i(\mu-\nu)} & e^{i\delta} & 1 \end{bmatrix} \tag{3.6}$$

In the matrix, terms (1,3), (3,1), (2,4) and (4,2) have the phase angle $\pm(\mu - \nu)$ and their interference patterns represent moire fringes of in-plane displacements. Terms (1,2),

(2,1), (3,4) and (4,3) have the phase angle $\pm\delta$ which are related to the difference of optical path length and are functions of the thickness of the air gap between the two grating surfaces. Terms (1,4), (4,1), (2,3) and (3,2) have the phase angle $\pm(\mu - v \pm \delta)$ and the corresponding interference pattern is a function of both parameters mentioned above.

When δ is no-zero, there are three different interference patterns formed on the image plane, and the moire fringes are hard to distinguish. If δ can be reduced to zero or very small, the second interference pattern could appear as a null-field with only intensity change, and the third one will have the same pattern as the first one which is the desired moire fringe pattern of in-plane displacements. The question is how to reduce the phase angle difference δ .

It is known that the phase angle difference δ is related to the difference of optical path length Δ by the equation

$$\delta = \frac{2\pi}{\lambda} \Delta_{OPL} \tag{3.7}$$

and the difference of optical path length Δ_{OPL} is a function of the thickness of the air gap d between the two grating surfaces. In the case of frequency mismatch (Fig. 3-9), it can be calculated as

$$\Delta_{OPL} = \{ [1 + \frac{1}{\cos\theta}] - [(\tan\theta + \tan\beta - \tan\alpha)\sin\alpha + \frac{1}{\cos\beta} + \frac{1}{\cos\alpha}] \} d \tag{3.8}$$

When θ = 49.43 deg., f_r = 1100 l/mm and f_s = 1200 l/mm, the result is $\Delta_{OPL} \simeq$ 0.008d.

In the case of rotational mismatch (Fig. 3-10), the difference of the optical path lengths can be calculated as

$$\Delta_{OPL} = [(1 + \sqrt{\tan^2\alpha + \frac{1}{\sin^2\theta}}) - (\frac{1}{\sin\theta} + \sqrt{1 + \tan^2\alpha})]d \qquad (3.9)$$

When θ = 49.43 deg., α = 5 deg. and $f_s = f_r$ = 1200 l/mm, the result is $\Delta_{OPL} \simeq$ 0.0009d.

According to the calculation by Eq. 3.8 and 3.9, the difference of the optical path length can be limited by reducing d, the thickness of the air gap. In the scheme of frequency mismatch, if the gap d is kept less than 30 wavelengths, the Δ_{OPL} is smaller than 1/4 wavelength, and the extraneous fringes will deviate the desired fringe pattern by 1/4 fringe order. This situation can be tolerated, the fringe pattern will have good contrast and the resultant pattern can be interpreted as the in-plane displacement pattern.

In the case of rotational mismatch, the difference of optical path lengths between the two diffraction orders (1,1,0 and 0,1,1) is much smaller (less than one thousandth of the thickness of d). If the thickness of the air gap between two grating surfaces can be kept less than 250 wavelengths, the desired fringe pattern will be deviated less than 1/4 fringe order. This condition offers more flexibility to the system. Larger specimens can be tested and more out-of plane deformation can be tolerated. Experiments have proved that the rotational mismatch can be used with up to one inch square testing area without any influence from the extraneous fringes. If the specimen surface is essentially flat and has only small out-of plane deformation during the test, this method can be used to measure even larger fields.

If one grating surface is tilted (by out-of-plane rotation) relative to the other, a small angular separation will appear between those two diffraction order sequences. However, this angular separation is so small that a very large tilting angle has to be used to separate the two beams properly. For example, with an out-of-plane tilt of 3 deg, the

two diffraction orders are separated by 0.5 deg. This is not a practical way to eliminate the extraneous fringes.

In both schemes, the null-field can be obtained and the carrier patterns can be introduced by adjusting the intersection angles between two incident beams and rotating the reference grating.

The two systems introduced above have high sensitivity to relative vibration of the two mirrors which direct incident beams B_1 and B_2 (Fig. 3-8). However, the separation between those two mirrors is very small, and the two incident beams travel very close to each other with a small intersection angle after they are separated. Moreover, a rigid fixture can be made to hold those two mirrors together with other optical elements, so that the relative vibration is extremely limited. In experimental verifications, there has been no problem to obtain a stable state for two incident beams if a small intersection angle is used.

Besides the property of low sensitivity to vibrations, the systems have another advantage. With an illuminating angle almost normal to the specimen surface, the incident beams can get into comparatively deep test areas without being blocked by the loading frames or the test structure itself. In many cases, it offers more flexibility in the design of experiments.

3.6.3 Scheme 3, a system using optical fibers

As discussed above, the sensitivity is a function of the intersection angle α between the incident beams. The smaller the angle α, the lower the sensitivity to vibrations. In order to reduce the angle α, optical fibers are used in the design of the system illustrated Fig. 3-12. Two optical fibers are fixed on a rigid fixture and relative movement is limited. Lens L_3 is used to collimate the two spherical beams coming from two optical fibers. It

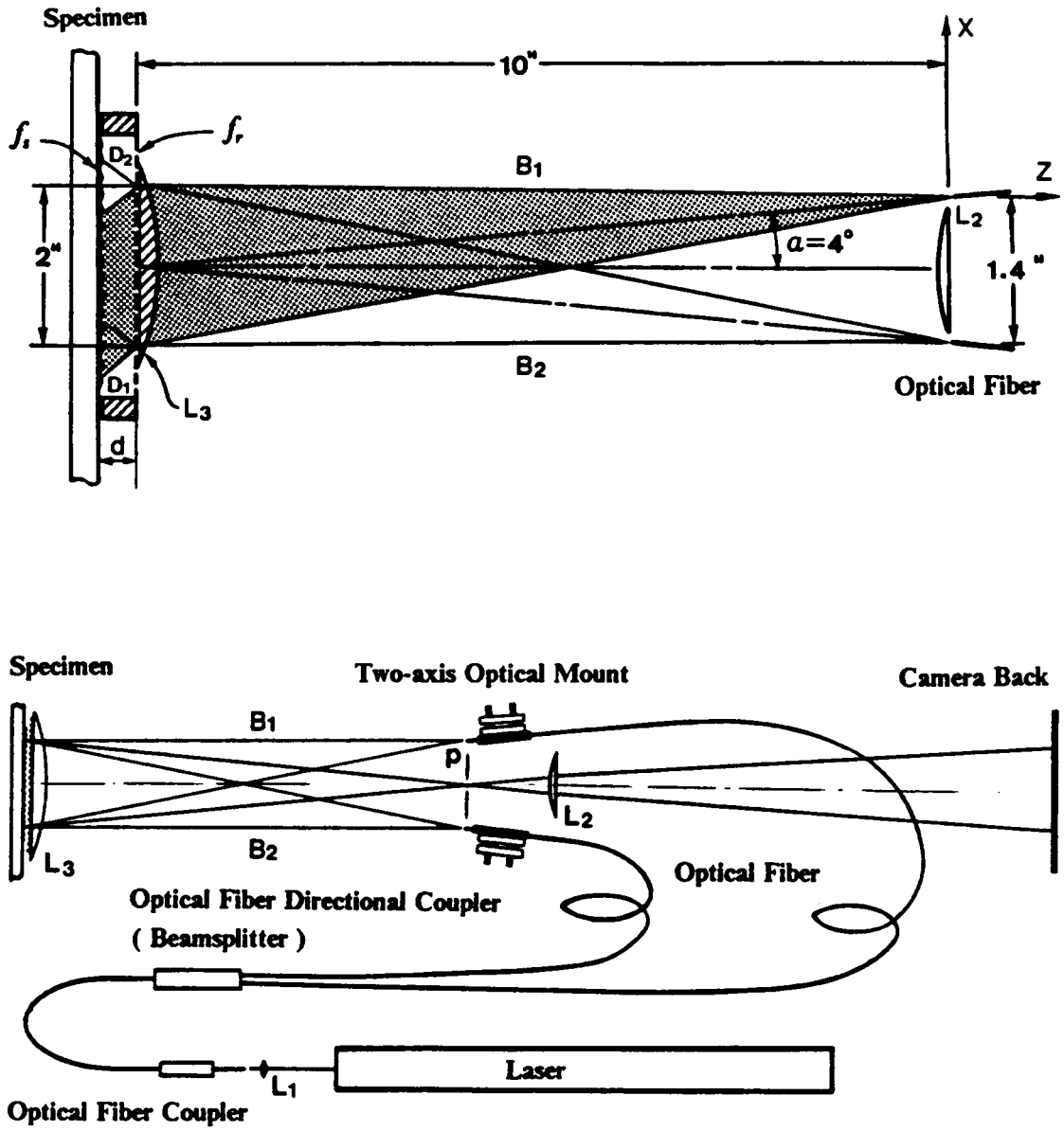

Fig. 3-12. A system using optical fibers to reduce the incidence angle. Frequency mismatch is applied. Sensitivity to vibrations is reduced by the small incidence angle α.

is also a field lens for photographing the fringe pattern on the specimen surface. The information beams collected by L_3 are focused on the plane P which contains the two fiber tips, so that the two optical fibers can be put very close to each other to reduce the incidence angle. A spatial filter is also located at the plane P to separate the information beam from the other optical noise. Lens L_2 is the camera lens which focus the image on the camera back. In this interferometer, the intersection angle can be reduced to less than 5 deg and the sensitivity to vibrations can be less than 10% of that obtained with the regular interferometer.

Both frequency and rotational mismatch can be applied in this system. However, a system with frequency mismatch has stricter requirement for the distance d between the reference grating and the specimen grating.

The relative vibration in the z direction between the two ends of the optical fibers would cause vibrations of fringe patterns. However, the distance between two fibers can be very small and the relative movements are easily eliminated by a rigid holder for two fiber ends. This system has the same problem of extraneous diffraction orders as the system discussed above. The collimating lens L_3 (with the real grating replicated on the flat side) has to be placed very close to the specimen surface. In practice, the lens is partially in contact with the specimen. The advantages, compared to the system with parallel incidence beams, are simplicity and compactness obtained by using optical fibers, also the high efficiency of light utilization.

In this system, null-field and carrier patterns can obtained by translating the ends of optical fibers, which is equivalent to adjusting the incidence angle of incident beams. A carrier pattern of extension will be introduced when the ends of optical fiber are translating in the direction perpendicular to the lines of the specimen grating. A carrier pattern of rotation will be introduced when one of the fiber end translates parallel to the grating lines relative to the other. A perfect null-field is hard to get because the inci-

dence beams D_1 and D_2 are not perfectly collimated. The reason is that the point light source from the tip of the optical fiber is not located on the optical axis of the collimate lens L_3. The optical distortion is more severe when a shorter focal length lens is used for collimating and the two tips of the optical fibers are more separated from the optical axis of the collimate lens. This is the shortcoming of the system.

3.6.4 Scheme 4, a two-beam system with zero incidence

The system is depicted in Fig. 3-13. Two pieces of linear reference grating, separated with a distance equal to the size of the specimen grating, are attached to the specimen. The camera is focused directly on the specimen surface through the gap between the two pieces of reference gratings. An important advantage of this system is that the beams go through the reference grating only once and the diffraction orders (1,1,0 and 0,1,1), which caused the problem in scheme 1 and 2, do not exist. A clean fringe pattern can be created.

A similar optical arrangement first appeared in the achromatic moire interferometer [20]. The purpose was to achieve equal optical path length for two incident beams in order to create optical interference for a incoherent light. By attaching the reference grating to the specimen, the system could be insensitive to the vibrations.

The distance between the reference gratings and the specimen grating is a function of the frequencies of the gratings and the angles of the incident beams. Zero incidence angle for two incident beams can be used to create the fringe patterns. Therefore, sensitivity to vibrations between the two beams and the reference grating is theoretically zero. Still, the high sensitivity has been preserved between the reference grating and the specimen grating where the deformations are measured. Because the system is still very sensitive to the relative movements between the reference grating and the specimen

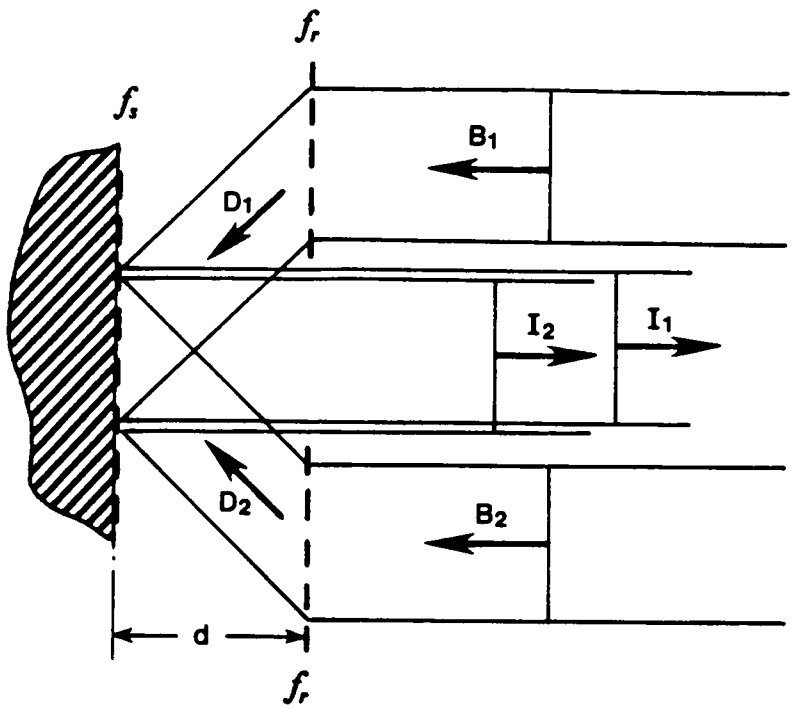

$$f_r = f_s = 1200 \ \textit{lines/mm}$$

Fig. 3-13. A system with zero deg incident beams. The real grating is attached to the specimen with a separation d.

grating, and the reference grating has to be placed a distance away from the specimen, a relatively rigid structure is necessary to hold the reference grating on the specimen. This might make the structure of the holder heavy and complicated.

This system also has full adjustability of null-field and carrier fringes, which is achieved by adjusting the intersection angle between the two incident beams and rotating the reference grating.

3.6.5 Scheme 5, a one-beam system with unsymmetrical incidence

A system with unsymmetrical illumination has a lot of advantages (Fig. 3-14). This system was developed from the real grating method published in the reference [10]. The difference is that the reference grating is attached to the specimen to minimize relative vibrations. By illuminating with a large angle β, the extraneous fringes, which were the severe problem in the first three schemes, can be completely eliminated. The old system uses one incidence beam and the frequency of the real grating was twice as high as the frequency of the specimen grating. Again, it does not have the abilities for adjusting the null-field and introducing carrier pattern of extension as the one beam system mentioned in scheme 1.

3.6.6 Scheme 6, the new two-beam system with unsymmetrical incidence

By using frequency mismatch or rotational mismatch techniques, the system can be developed into a two beam system (Fig. 3-15). One beam (from the full mirror M_2) strikes the reference grating with an angle β and the other one (from the partial mirror) has a small deviation α . The reference grating used here has a frequency of 2300

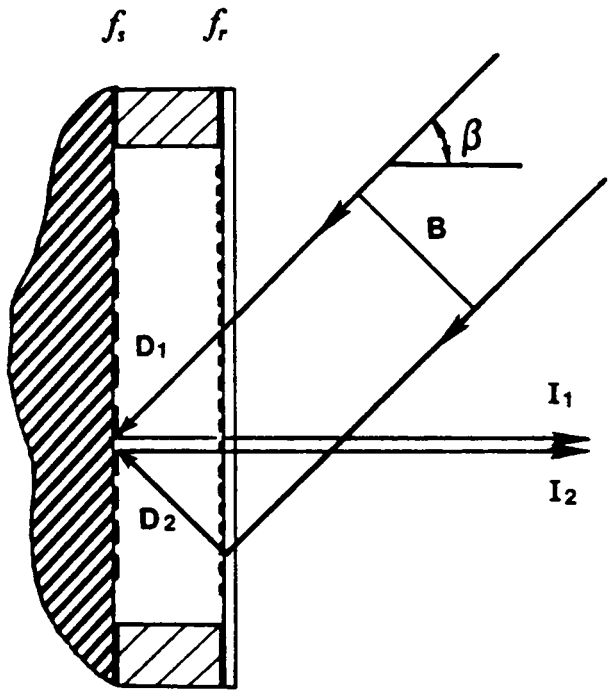

$$f_r = 2400 \ lines/mm$$

$$f_s = 1200 \ lines/mm$$

Fig. 3-14. Schematic ray diagram of a system using a real grating and a unsymmetrical incidence beam.

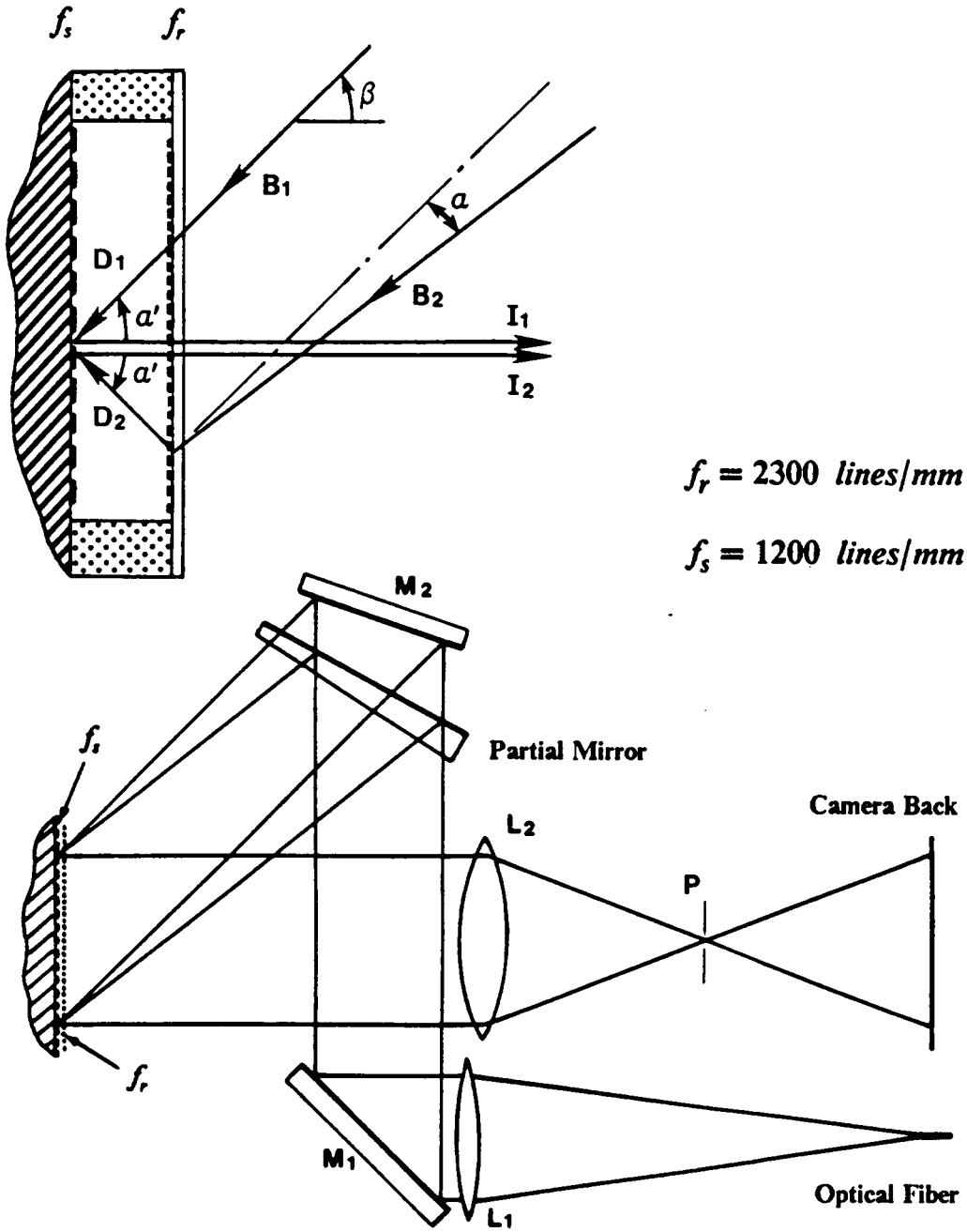

Fig. 3-15. Diagrams of the unsymmetrical system with two incident beams. Frequency mismatch is applied.

lines/mm and the angle α is 5.2 deg when the wavelength is 633 nm and the angle β is 49.4 deg. Only one diffraction order from each incident beam can enter the camera. This system does not have the problem of extraneous diffraction orders as in the case of the first three schemes. The air gap d between the two grating surfaces is not critical to the quality of the fringe patterns, and large specimens and high out-of plane deformations can be tolerated. The information beams emerge from the specimen surface with diffraction angles different from the angles of directly reflected beams and the other diffraction orders, and by using a spatial filter at plane P, they can be well separated. The intensity of the two information beams can be equalized by choosing the transmission and reflection ratio of the partial mirror to optimize the contrast of fringe patterns. The camera lens can be placed very close to the specimen to achieve the large numerical aperture and the magnification. The lower sensitivity to vibrations can be obtained in the new system, compared to the symmetric systems shown in scheme 1 and 2, if the incidence angle α is further reduced.

By using optical fiber to transmit the laser light, the interferometer can be separated from the light source. Since few optical elements are used in this system, it is possible to build a portable system from this design.

Because of the absence of the extraneous diffraction orders, the extraneous fringes created by the air gap d are no longer an important factor of consideration, and both frequency mismatch and rotational mismatch can be used to obtain high quality fringe patterns. However, the frequency mismatch seems preferable because of the easier alignment of the optical system.

This system seems to be the best solution for the objective of a vibration insensitive system. The other systems mentioned above have their own advantages and disadvantages. Each one can be used in different cases and perform some special functions. However, the last system is the one recommended to deal with the vibration problems

and perform moire interferometry off the optical table. It has all the properties that the regular moire interferometer has but does not have any significant limitations.

The schematic diagram of the unsymmetrical system in Fig. 3-15 shows a linear system measuring one displacement field only. The system can be expanded to a two-dimensional system to measure x and y direction displacements fairly easily because the principle is the same. In a two-dimensional system, more optics are needed and cross gratings have to be used for both specimen and reference grating.

3.7 Experimental Evaluations

3.7.1 Nonuniformities in composites by the three mirror system

As an application of new moire interferometers, the strain nonuniformities in graphite/epoxy panels were investigated. The specimens were tensile strips cut from those composite panels (Fig. 3-16a). High loading was required to expose the nonuniformities in the interior of the materials, and the tests had to be performed on the testing machine. The interferometer used was the three mirrors system. Its self compensation property eliminates the linear vibrations from the testing machine. The interferometer was attached to the specimen. Carrier patterns were introduced for each loading step to cancel the uniform part of the strains, and the fringe patterns were recorded. As mentioned before, this technique cannot be used to measure the absolute strains. The uniform part of the strains was measured by a strain gauge fixed on the back of each specimen. The fringe patterns presented the nonuniform part of the strain distributions, which was the desired parameter. In order to determine the signs of fringe gradients, a

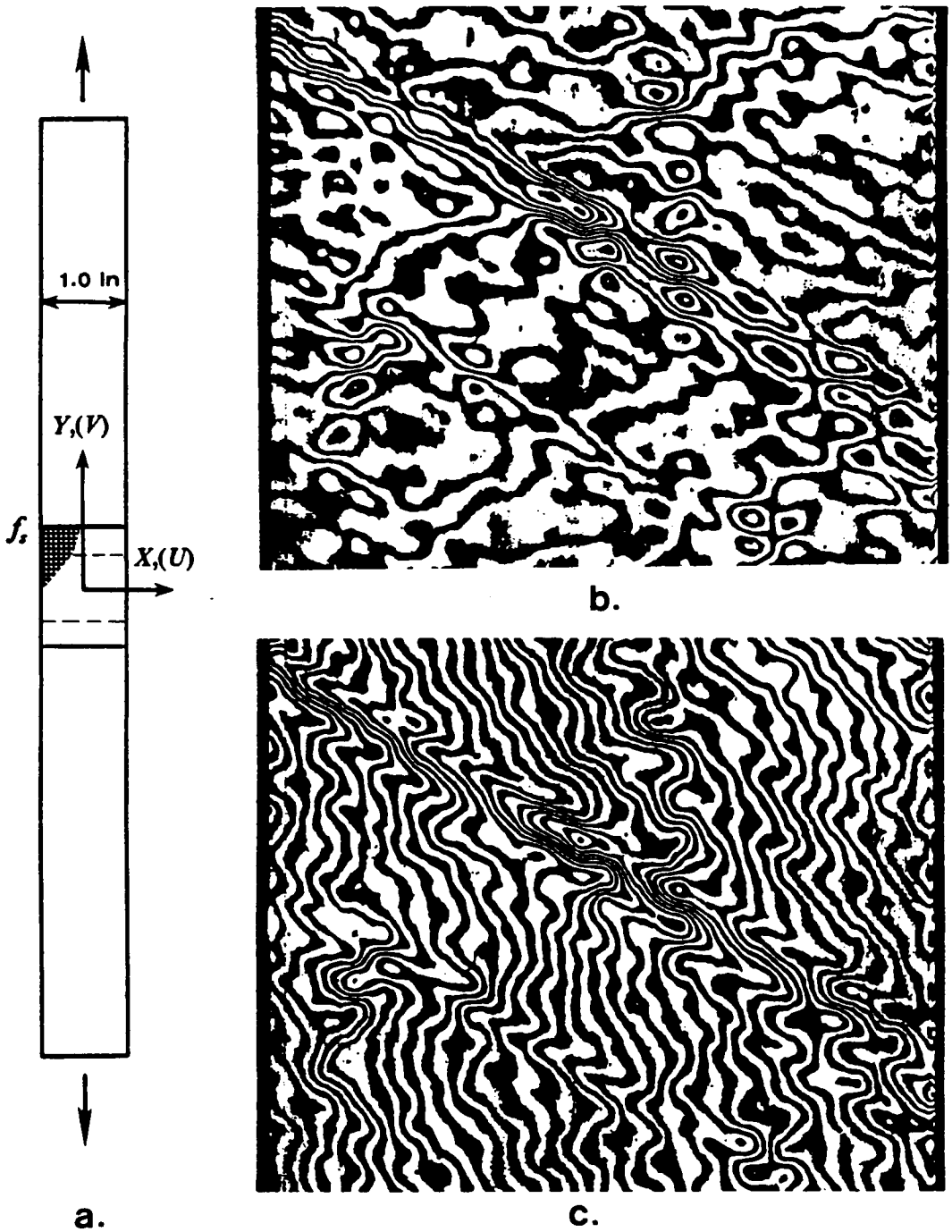

Fig. 3-16. Nonuniformities in graphite/epoxy composite by the three mirror system attached to the specimen. a. Specimen and loading. b. U field with average strain cancelled. c. Same U field with carrier fringes of known sign added.

small frequency carrier fringes with a known sign were introduced. Figure 3-16c is the fringe pattern of U displacement field with carrier fringes.

The specimen had 16 layers and a stacking sequence of [0/60/-60/90/90/-60/60/0]s. As shown in Fig. 3-16b and c, the strain concentrations in the 60 deg layer, which was the second layer from the top surface, is very high even though the measurement is made on the outer surface. The magnitude of the nonuniformity part of the strains was about 35% of the average strain. A comprehensive report is given in Ref.[7].

The technique was very successful in moving moire interferometry off the optical table. Clear fringe patterns were obtained in both U and V displacement fields when the specimens were loaded in a regular testing machine. However, there are some drawbacks of this technique. First, it cannot be used to measure the absolute strains, which are very important in many cases of investigating the properties of materials. Second, the interferometer contains three mirrors which are heavy enough to influence the strain distributions on specimens in certain circumstances.

3.7.2 System using optical fibers

Figure 3-17 shows the experiment result of the system introduced as scheme 3. The experiment was performed on a screw-driven testing machine without any vibration isolation. The specimen was a graphite-epoxy composite strip with a central hole, and the staking sequence was $[0_2/\pm 45/90]$s. A plano-convex lens with a reference grating replicated on the flat side was attached to the specimen. The air gap between the reference grating and specimen grating was minimized, but a small in-plane movement was allowed between the two gratings.

The rotational mismatch was applied, and the system was tuned to obtain the fewest fringes in the initial fringe pattern. A tensile load was applied to investigate the strain

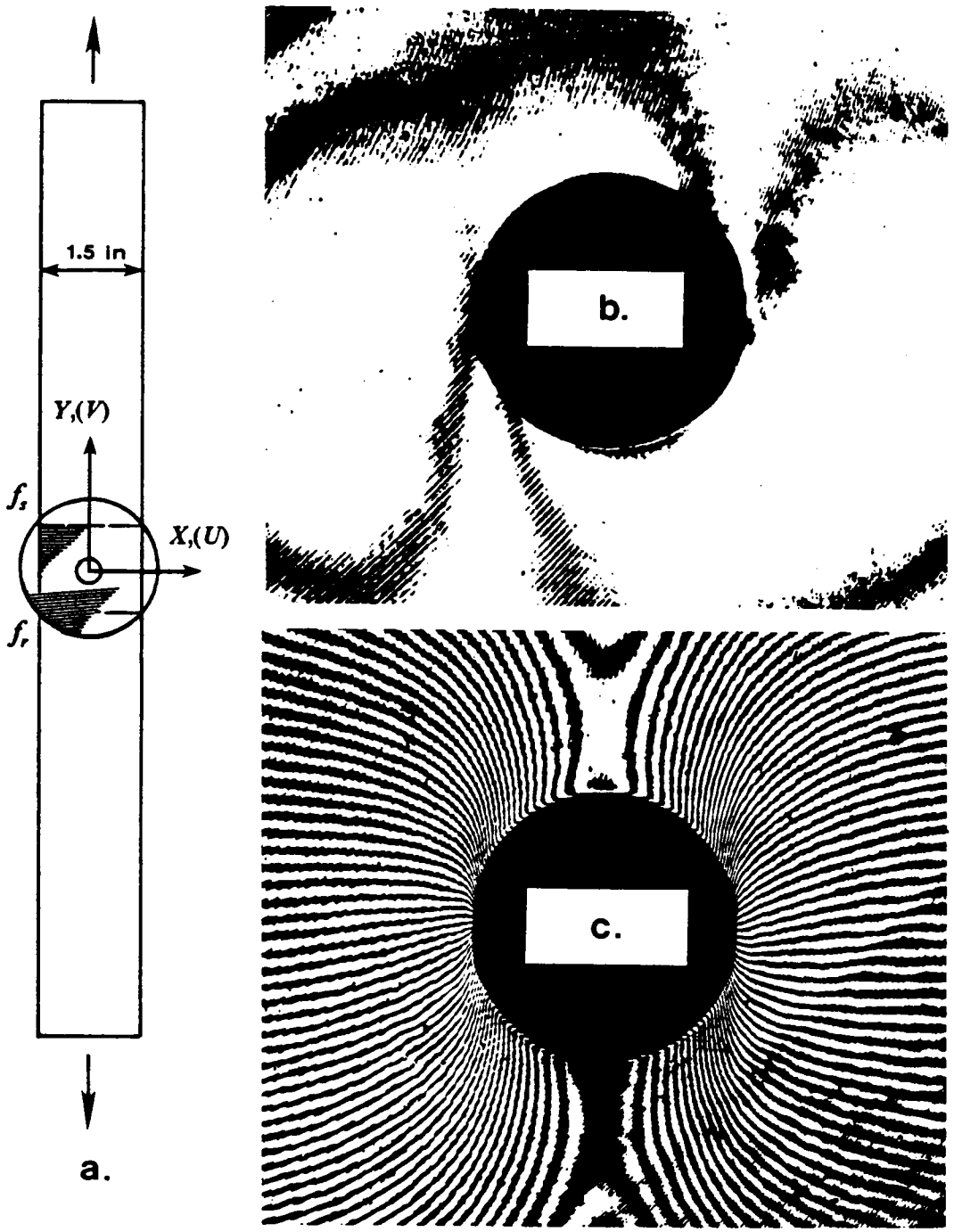

Fig. 3-17. Application of the system with optical fibers (scheme 3) with rotational mismatch. a. The specimen and the attached collimating lens reference grating replicated on it. b. V displacement field of zero load (null-field). c. V displacement field with tensile load.

concentrations introduced by the central hole. Figure 3-17 shows the V (vertical) displacement fields before and after the specimen was loaded. By using a long focal length lens (f= 11 in), the optical distortion was minimized.[8] In a 3/4 by 3/4 in area, the initial pattern (null-field) had only three fringes which was negligible when the high strain concentrations were considered. The maximum shear strain measured in the fringe pattern in Fig. 3-17 is 0.76 percent strain. At this high strain level, the interferometer still offered high quality fringe patterns.

The other displacement field, U field, can be obtained by duplicating the experimental procedure in the horizontal direction. Because few optical elements are used in this system, it is easier to build a separate system for the U displacement field instead of making use of the light from the V field. Usually if a system is operating for one field measurement, it can be expanded to measure the other field without any trouble. For a two-direction measurement, cross-line gratings have to be used for both specimen and reference grating [20].

3.7.3 Unsymmetrical system on a hydraulic testing machine

A system similar as the one in Fig. 3-15 was built to perform a test on a hydraulic testing machine which usually has more severe vibrations than a screw-driven testing machine. The frequency mismatch was used and a reference grating with 2274 line/mm was attached to the specimen (Fig. 3-18). As shown in Fig. 3-15, a collimated beam was reflected by a full mirror and a partial mirror to illuminate the reference gratings. The two incidence beams had a very small intersection angle, and the sensitivity to vibrations was very small (about 10% of the regular moire system).

---

[8] The optical distortion was caused mainly by the off axis illumination as mentioned in section 3.6.3.

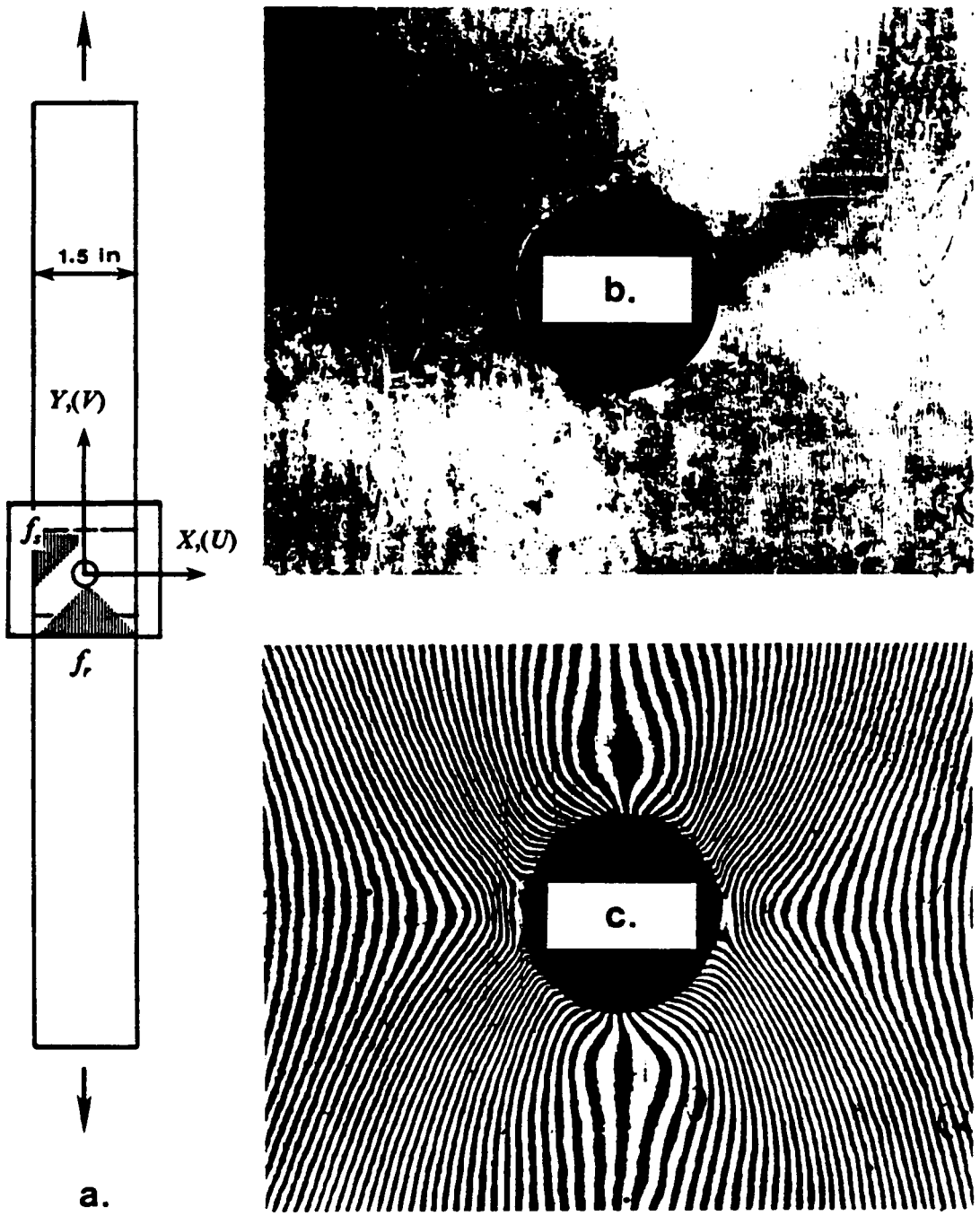

Fig. 3-18. Application of the unsymmetrical system (scheme 6) with frequency mismatch. a. Specimen and loading. b. The fringe pattern of the U displacement field with zero load. c. The fringe pattern of the U displacement field with the applied tensile load.

The specimen was a graphite-epoxy composite strip with a central hole similar to the one tested by the system of scheme 3, but had a staking sequence of $[0/\pm 45_4/90]s$. The measurement was made under steady loads and sequential loads to test the performance of the system under a vibration condition. The pictures of fringe patterns were recorded during the experiments. Under both loading situations, the fringe patterns were very stable and had very good contrast. Fig. 3-18 shows the fringe patterns of the U displacement fields obtained when the sequential load was applied. The rate of loading was 15 lb/sec., and the two pictures were taken at 0 and 1500 lb load.

Figure 3-19 shows the photograph of the experiment. The whole interferometer is built on a 12x24 in aluminum plate, and supported by a tripod. The optical set up is simple and easy to be installed. Because of the low sensitivity to vibrations, the interferometer can be operated off the optical table in a comparatively rough environment. Pictures of the moire fringe patterns can be taken under the regular room light by using a 35mm camera back.

As mentioned in section 3.6.6, the system can be easily developed to a two-dimensional system to measure both U and V displacement fields. Cross-line gratings for both reference and specimen grating have been used in the previous experiments of the unsymmetrical system. But the optical system in Fig. 3-19 has to be expanded slightly to build a two-dimensional interferometer.

3.8 Conclusions of chapter 3

For a long period, the applications of moire interferometry have been limited to the optical table because of vibration problems. The capacities of loading devices and other conditions in an optical laboratory restricted experiments to small specimens and sam-

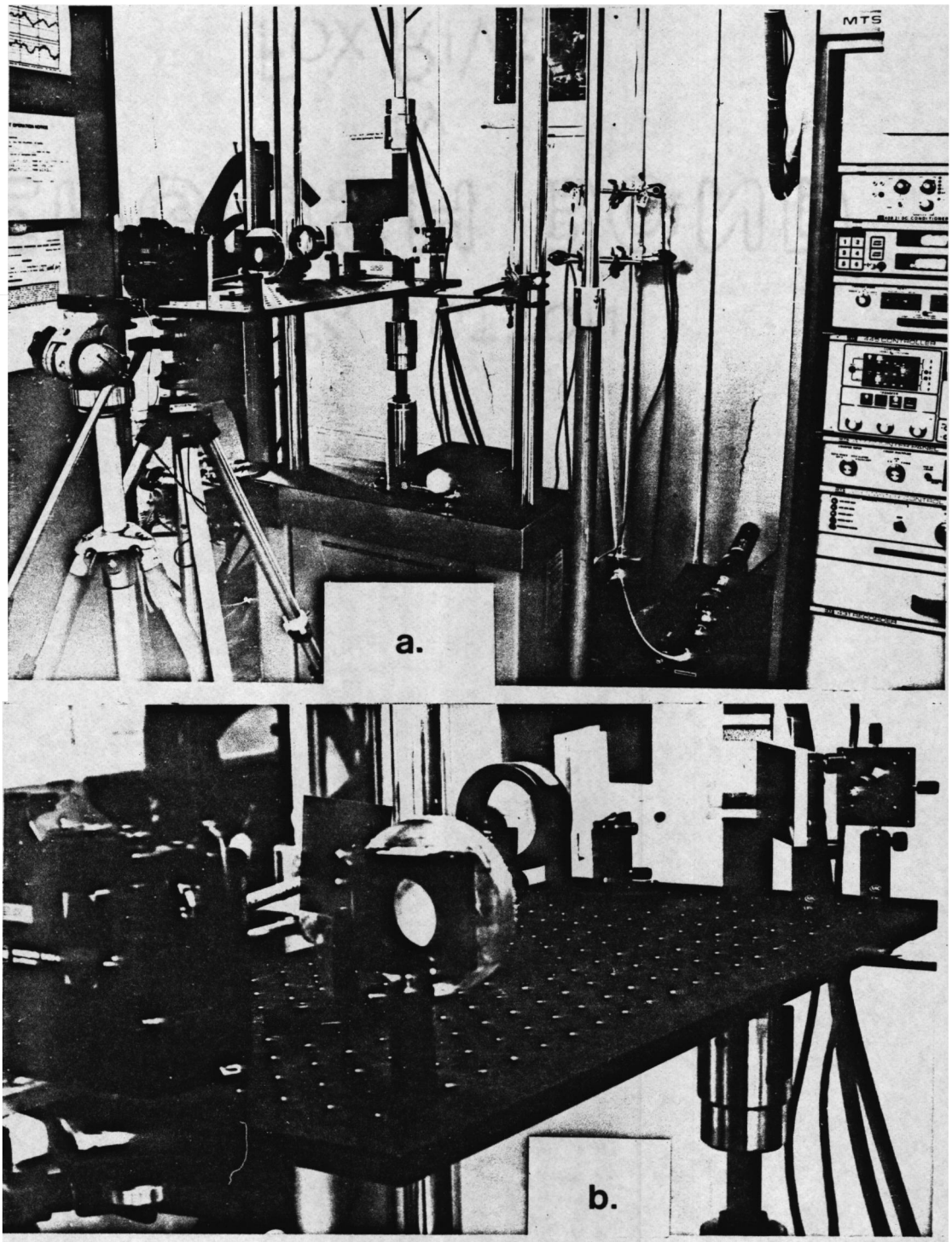

Fig. 3-19. The experiment of the unsymmetrical system. a. The setup on a hydraulic testing machine. b. The unsymmetrical system of moire interferometry.

ples. Structures and large specimens were rejected by the limitations of moire system. By moving moire interferometry off the optical table, the applications of moire interferometry can be vastly increased.

By attaching certain optical elements to the specimen, the sensitivity to vibrations can be greatly reduced. These optical elements could be mirrors, real gratings or prisms. The systems can be moved off the optical table to measure large structures and specimens on testing machines or to perform experiments in a rough environment.

The systems introduced have all the adjustabilities as the regular moire system, and carrier patterns are easily introduced. Most of them have very simple structures, and can be built as portable systems.

For many problems, the system introduced as scheme 6 is the best of those proposed. It is very practical system with simple optical structure and few optical elements. The system can be set up easily on testing machines and other field conditions. It is an ideal vibration insensitive moire system for performing off-table measurements.

4.0 References

1. S. W. Tsai, H. T. Hahn, "Introduction to Composite Materials," Technomic Publishing Co. Inc. , 1980.

2. R. M. Jones, "Mechanics of Composite Materials," Scripta Book Company, Washington D. C.

3. M. J. Salkind, G. S. Holister, "Applications of Composite Materials," ASTM Special Technical Publication #524.

4. D. Post, R. Czarnek, "Experimental Studies of Fiber Reinforced Composite Materials and Structures," Progress Report, May, 1987.

5. D. Post, "The Analysis of Deformations and Strains in Composites by Moire Interferometry," *Proceedings of the Sixth International Conference on Composite Materials and Second European Conference on Composite Materials,* F. L. Matthews, N. C. R. Buskell, J. M. Hodgkinson and J. Morton, editors, Elsevier, NY, Vol. 5, 1987.

6. D. Post, "Advances in Moire Interferometry," pp. 39-46, *Photoelasticity,* M. Nisida, editor, Springer-Verlag, Tokyo, New York, 1986.

7. R. Czarnek, D. Post, Y. Guo, "Nonuniformaties in Composite Panels by Moire Interferometry," *Proceedings of the 1986 SEM Spring Conference on Experimental Mechanics,* SEM, Bethel, CT, June, 1986.

8. R. Czarnek, D. Post, Y. Guo, "Strain Concentration Factors in Composite Materials," *Proceedings of the 1986 SEM Conference,* New Orland, June, 1986.

9. R. Czarnek, D. Post and C. T. Herakovich, "Edge Effects in Composites by Moire Interferometry," *Experimental Techniques,* Vol. 23(1), Jan. 1983.

10. D. E. Bowles, D. Post, C. T. Herakovich and D. R. Tenney, "Moire Interferometry for Thermal Expansion of Composites," *Experimental Mechanics,* Vol. 21, No. 12, Dec. 1981.

11. P. Ifju, D. Post, "Thermal Strain Analysis Using Moire Interferometry," *Proceedings of SPIE - The International Society for Optical Engineering,* Vol. 814, Part 2, San Diego, California, Aug. 1987.

12. D. Post, F. L. Dai, Y. Guo and P. Ifju, "Interlaminar Shear Moduli of Cross-Ply Laminates: An Experimental Analysis," Submitted to *Journal of Composites Technology and Research.*

13. D. Post, R. Czarnek and D. Joh, "Shear Strain in a Graphite-PEEK Beam by Moire Interferometry with Carrier Fringes", *Experimental Mechanics,* Vol. 27, pp. 246-249, Sept. 1987.

14. R. Czarnek, Y. Guo, K. D. Bennett and R. O. Claus, "Interferometric Measurements of Strain Concentrations Induced by an Optical Fiber Embedded in Fiber Reinforced Composites," *Proceedings of SPIE International Symposium and Exhibition on Fiber Optics, Optoelectronics and Laser Applications,* Boston, Mass., Sept. 1988.

15. Y. Wang, "Interlaminar Compression of Thick Composites," *Engineering Mechanics, 7th Conference Abstracts,* Blacksburg, VA, May, 1988.

16. D. Joh, "An Experimental Study of Frictional Phenomena Around the Pin Joints of Plates Using Moire Interferometry," *Ph.D Dissertation in Virginia Polytechnic Institute and State University,* Dec. 1986.

17. D. Post, R. Czarnek, D. Joh, J. Jo and Y. Guo, "Deformation of a Metal-Matrix Tensile Coupon with a Central Slot: An Experimental Study," *Journal of Composites Technology and Research,* Vol. 9, No. 1, Spring, 1987.

18. D. Post, R. Czarnek, D. Joh, J. Jo and Y. Guo, "Experimental Study of a Metal-Matrix Composite," *Experimental Mechanics,* Vol. 27, No. 2, pp. 190, June, 1987.

19. Y. Guo, D. Post, R. Czarnek, "Deformation Analysis of a Metal Matrix Composite by Moire Interferometry," *Proceedings of the CCMS (Center for Composite Materials and Structures) Fourth Annual Review,* May, 1987.

20. D. Post, "Moire Interferometry," Chap. 7, *Handbook of Experimental Mechanics,* A. S. Kobayashi, Editor, Prentice-Hall, Englewood Cliffs, NJ, 1987.

21. R. Czarnek, "New Methods in Moire Interferometry," *Ph.D Dissertation in Virginia Polytechnic Institute and State University,* Dec. 1984.

22. D. Post, "Moire Fringe Multiplication with a Nonsymmetrical Doubly Blazed Reference Grating," *Applied Optics,* Vol. 10, pp. 901, April, 1971.

23. D. Post and W. A. Baracat, "High-sensitivity Moire Interferometry -A Simplified Approach," *Experimental Mechanics,* Vol. 21, No. 3 , pp.100, March, 1981.

24. D. Post, "Moire Interferometry at VPI & SU," *Experimental Mechanics,* Vol. 23(2), pp. 203-210, June, 1983.

25. D. Post, "Optical Interference for Deformation Measurements - Classical, Holographic and Moire Interferometry," *Mechanics of Nondestructive Testing,* Proceeding edited by W.W. Stinchcomb, Plenum Publishing Corp., New York, 1980.

26. A. Livnat and D. Post, "The Governing Equations for Moire Interferometry and Their Identity to Equations of Geometrical Moire," *Experimental Mechanics,* Vol. 25, No. 4, Dec. 1985.

27. F. Mirzadeh, K. L. Reifsnider and Y. Guo, "Micro-deformation and Failure Mode of Woven Composites in Compression," *Proceedings of the CCMS Fifth Annual Review,* Blacksburg, VA, Apr. 1988.

28. Fu-Pen Chiang, "Moire Method of Strain Analysis," Chap. 6, *Manual on Experimental Stress Analysis,* A. S. Kobayashi, Editor, Society for Experimental Stress Analysis, Bethel, CT, 1978.

29. R. Czarnek and D. Post, "Moire Interferometry with +45-deg Gratings," *Experimental Mechanics,* Vol.24, No.1, March, 1984.

30. D. Post, "Moire Interferometry, 1986," 10th Nat'l. Congress on Applied Mechanics, Austin, Texas, June, 1986.

31. V. J. Parks, "Geometric Moire," Chap. 6, *Handbook of Experimental Mechanics,* A. S. Kobayashi, Editor, Prentice-Hall, Englewood Cliffs, NJ, 1987.

32. Y. Guo, D. Post, R. Czarnek, "The Magic of Carrier Pattern in Moire Interferometry," *Experiment Mechanics,* (to be published).

33. J. Mckelvie, C. Walker, P. Mackenzie, "A Workaday Moire Interferometer: Conceptual and Design Considerations; Operation; Applications; Variations; Limitations," *Proceedings of SPIE Conference,* Vol. 814-2, Aug. 1987.

34. V. A. Deason, J. Epstein and W. G. Reuter, "A Dynamic Moire Interferometry Technique," *Proceedings of 1985 SEM Conference on Experimental Mechanics,* Las Vagas, June, 1985.

35. D. Post, "Moire Interferometry with White Light," *Applied Optics,* Vol. 18, pp. 4163, Dec. 1979.

36. R. Czarnek, "Moire Interferometry with Chromatic Light," SPIE Vol. 679, Current Developments in Optical Engineering and Diffraction Phenomena, 1986.

37. D. Post, "Developments in Moire Interferometry," *Optical Engineering,* Vol. 21(3), pp. 458-467, May, 1982.

5.0 Figure Captions

Fig. 1-1. Shear strain measured by moire interferometry, a. Moire interferometry fringe pattern depicting the y-displacement field for a metal-matrix composite specimen with a center slot. b. Shear strain distribution along line L.

Fig. 1-2. The principle of the geometric moire method

Fig. 1-3. Moire interferometry and relevant equations

Fig. 1-4. The rigorous explanation of moire interferometry by the diffraction theory. a. Schematic ray diagram of moire interferometry. b. Diffraction beams produced by the specimen grating. The plus and minus first diffraction order I_1 and I_2 from two incidence beams B_1 and B_2 form a fringe pattern on the camera back.

Fig. 1-5. Moire fringe patterns are contour maps of the U and V components of displacement. The pictures were obtained from a test of a graphite/epoxy woven composite specimen, loaded in compression along its y axis [15].

Fig. 1-6. The sensitivity resolution is the displacement represented by half fringe order, The center lines of dark and bright fringes are used as the accurate data points.

Fig. 1-7. The range of measurement, strain variation, from zero strain to + 0.056 strain, is recorded in the same fringe pattern. The derivative $\frac{\partial V}{\partial x}$ is obtained from this pattern of the V field. In the corresponding U field, the derivative $\frac{\partial U}{\partial y}$ is negligibly small.

Fig. 1-8. Displacement components and boundary conditions. a. If only the magnitudes of U and V displacements are known, there are four possibilities for the displacement at an arbitrary point A. Two boundary conditions have to be applied to determine the true displacement, e.g. $u > 0$ and $v < 0$. b. If the magnitude of displacement component is known in third direction, e.g. U_{45}, the boundary condition can be reduced to only one, e.g. $u > 0$.

Fig. 2-1. The distributions of displacement between two neighboring fringes

Fig. 2-2. Fringe azimuth and fringe vectors

Fig. 2-3. The carrier fringes of rotation. a. The carrier fringes of rotation introduced by the relative rotation of angle γ between the specimen grating and the refer-

ence grating. b. The gradient of carrier fringes of rotation has two components, the desired carrier fringes F_c and the extraneous fringes F_e.

Fig. 2-4. Interlaminar shear test of [90/90/0]n graphite/epoxy composite specimen, a. the load-induced fringes of V displacement field, b. the shear strain distribution along a horizontal line across the specimen. Since $\partial U / \partial y = 0$ along this line, the shear strain the data is extracted directly from pattern (a). The insert at the bottom is a photograph showing the ply sequence.

Fig. 2-5. Carrier fringes are used to increase the resolution of fringe gradients in the test of Fig.2-4. a. Load-induced fringes with carrier fringes of extension. The slopes show the shear strain levels. b. Actual strain distribution, which reveals high shear strains in the resin-rich zones between plies.

Fig. 2-6. Five-point bending beam test of [+45/0/-45/90]6s graphite-PEEK composite specimen. a. Specimen and loading. b. Load-induced fringe pattern of the U field for the portion of the specimen in dashed box. c. Load-induced fringes with carrier pattern of extension. d. Shear strain distribution along the line A-A'

Fig. 2-7. Interlaminar compression test of [90/90/0]n graphite/epoxy composite specimen. a. Load-induced fringe pattern of the V field for portion of the specimen in dashed box, b. Load-induced fringes with carrier fringes of extension and rotation. c. The vector diagram. d. Apparent strain distribution (the dashed curve), which dose not show the existing strain concentrations and the Actual strain distribution (the solid curve), which reveals the high compressive strains in the resin-rich zones between plies.

Fig. 3-1. Optical setup of a linear moire system, where the specimen is separated from the optical table.

Fig. 3-2. Rigid body motions between the specimen grating and the virtual reference grating are the three translations (x, y, z) and the three rotations (ϕ_x, ϕ_y, ϕ_z).

Fig. 3-3. Sensitivities of a moire system to the rotations of the specimen grating.

Fig. 3-4. The sensitivity of a moire system is a function of the incidence angles of two coherent beams which create the reference grating. a. A regular moire system, where the incidence angles are 49.4 deg and sensitivity is 0.417 micrometer per fringe order. b. A moire system with reduced sensitivity, where the incidence angles are smaller.

Fig. 3-5. An attached optical element can be used to redirect the incident beams and reform the high sensitivity for measurement

Fig. 3-6. A three mirror moire system, mirrors are attached to the specimen to reduce the influence of vibrations.

Fig. 3-7. Schematic ray diagram of a one-beam system with normal incidence.

Fig. 3-8. Diagrams of a two-beam system with symmetric incidence.

Fig. 3-9. Schematic ray diagrams for the new two beam system with frequency mismatch. By using symmetric beams with incidence angles of 5 deg, the sensitivity to the vibration is reduced to 11% of the regular moire interferometer.

Fig. 3-10. Schematic ray diagrams of the new two-beam system with rotational mismatch. The sensitivity of vibrations is reduced when the small incidence angle α is used.

Fig. 3-11. The four diffraction beams from incidence beams, B_1 and B_2 will enter the camera. Two of them B_{11} and B_{21} interfere to form moire fringe pattern. Extraneous fringe patterns (noise) are added to the moire pattern because of the present of the diffraction orders B_{12} and B_{21}.

Fig. 3-12. A system using optical fibers to reduce the incidence angle. Frequency mismatch is applied. Sensitivity to vibrations is reduced by the small incidence angle α.

Fig. 3-13. A system with zero deg incident beams. The real grating is attached to the specimen with a separation d.

Fig. 3-14. Schematic ray diagram of a systems using real gratings and unsymmetrical incident beam.

Fig. 3-15. Diagrams of the unsymmetrical system with two incident beams. Frequency mismatch is applied.

Fig. 3-16. Nonuniformities in graphite/epoxy composite by the three mirror system attached to the specimen. a. Specimen and loading. b. U field with average strain cancelled. c. Same U field with carrier fringes of known sign added.

Fig. 3-17. Application of the system with optical fibers (scheme 3) with rotational mismatch. a. The specimen and the attached collimating lens reference grating replicated on it. b. V displacement field of zero load (null-field). c. V displacement field with tensile load.

Fig. 3-18. Application of the unsymmetrical system (scheme 6) with frequency mismatch. a. Specimen and loading. b. The fringe pattern of the U displacement field with zero load. c. The fringe pattern of the U displacement field with the applied tensile load.

Fig. 3-19. The experiment of the unsymmetrical system. a. The setup on a hydraulic testing machine. b. The unsymmetrical system of moire interferometry.

Appendix A. The Two Components of Carrier Fringes of Rotation

When carrier fringes of rotation are introduced, two components of fringe gradient are added to the fringe pattern. F_c is the desired component of the carrier fringes of rotation, and it lies parallel to the specimen grating lines. F_e is the extraneous component, and it lies perpendicular to the specimen grating lines.

As shown in Fig. 2-3, in the triangle ABC,

$$\sin\gamma = \frac{1/f}{1/F_c} = \frac{F_c}{f}$$

Thus $F_c = f \sin\gamma$. Since γ is very small, substituting γ for $\sin\gamma$, we have

$$F_c = \gamma f \qquad (a)$$

in the triangle ABD

$$\tan\frac{\gamma}{2} = \frac{1/F_c}{1/-F_e} = \frac{-F_e}{F_c}$$

Thus $F_e = -F_c \tan\frac{\gamma}{2}$. Since γ is very small, then $F_e = -F_c\frac{\gamma}{2}$. Hence, substituting F_c from Eq. (a), we obtain

$$F_e = \frac{-\gamma^2 f}{2} \tag{b}$$

The negative sign of F_e is determined by the sign of equivalent normal strain introduced. For a fixed coordinate system aligned with the initial orientation of the specimen grating lines, the extraneous component F_e is always negative because it introduces apparent uniform compressive strain on the specimen surface.

The vita has been removed from the scanned document